Performance Evaluation of a Solar ORC System Using Evacuated Flat Plate Photovoltaic-Thermal Collector as an Evaporator

By

Izaz Ahmad Qureshi

Reg#00000203669

Session 2017-19

Supervised by

Prof. Dr. Adeel Waqas

A Thesis Submitted to the US-Pakistan Center for Advanced Studies in Energy in partial fulfillment of the requirements for the degree of

MASTERS of SCIENCE in

ENERGY SYSTEMS ENGINEERING

US-Pakistan Center for Advanced Studies in Energy (USPCAS-E)

National University of Sciences and Technology (NUST)

H-12, Islamabad 44000, Pakistan

January 2020

Performance Evaluation of a Solar ORC System Using Evacuated Flat Plate Photovoltaic-Thermal Collector as an Evaporator

By

Izaz Ahmad Qureshi
Reg # 00000203669
Session 2017-2019

Supervised by
Prof. Dr. Adeel Waqas

A Thesis Submitted to the US Pakistan Centre for Advanced Studies in Energy in partial fulfillment of the requirements of the degree of

MASTER of SCIENCE
in
ENERGY SYSTEMS ENGINEERING

US-Pakistan Centre for Advanced Studies in Energy (USPCAS-E)
National University of Sciences and Technology (NUST)
H-12, Islamabad 44000, Pakistan

January, 2020

THESIS ACCEPTANCE CERTIFICATE

Certified that final copy of MS/MPhil thesis written by Izaz Ahmad Qureshi (Registration No. 00000203669), of U.S.-Pakistan Centre for Advanced Studies in Energy has been vetted by undersigned, found complete in all respects as per NUST Statues/Regulations, is within the similarity indices limit and accepted as partial fulfillment for the award of MS/MPhil degree. It is further certified that necessary amendments as pointed out by GEC members of the scholar have also been incorporated in the said thesis.

Signature: _____

Name of Supervisor _____

Date: _____

Signature (HoD): _____

Date: _____

Signature (Dean/Principal): _____

Date: _____

Certificate

This is to certify that work in this thesis has been carried out by **Mr. Izaz Ahmad Qureshi** and completed under my supervision in, US-Pakistan Center for Advanced Studies in Energy (USPCAS-E), National University of Sciences and Technology, H-12, Islamabad, Pakistan.

Supervisor: _____

Dr. Adeel Waqas
USPCAS-E
NUST, Islamabad

GEC member # 1: _____

Dr. Majid Ali
USPCAS-E
NUST, Islamabad

GEC member # 2: _____

Dr. Adeel Javed
USPCAS-E
NUST, Islamabad

GEC member # 3: _____

Dr. Nadia Shahzad
USPCAS-E
NUST, Islamabad

HoD- Energy Systems Engineering: _____

Dr. Naseem Iqbal
USPCAS-E
NUST, Islamabad

Principal/ Dean: _____

Dr. Adeel Waqas
USPCAS-E
NUST, Islamabad

List of Publications

1. Izaz Ahmad, Adeel Waqas "Performance evaluation of an evacuated flat plate photovoltaic-thermal (PVT) collector for heat and electricity" International Conference on Emerging Technologies 2019, FAST NUCES, Peshawar. doi: 10.1109/ICET48972.2019

Acknowledgement

I am grateful to Dr. Adeel Waqas for supervising my research, guiding me during the course of my research work and providing constant feedback to improve it. I would like to thank USPCAS-E NUST and USAID for providing me the platform and sponsored my research work. I am also grateful to faculty members of USPCAS-E NUST for their efforts in teaching us coursework during post-graduate program of Energy Systems Engineering. I would also like to express my gratitude to my colleagues, graduate scholars and friends for their academic support. Last but not the least, I am thankful to my parents, family and friends for their constant moral support.

Contents

List of Figures

List of Tables

Nomenclature

A	area	m^2
Bo	boiling number	-
Co	convection number	-
C_b	bond conductance	
C_p	specific heat	J/kg K
D	diameter	m
FPC	flat plate collector	-
FPV-T	flat plate photovoltaic thermal collector	-
EFPV-T	evacuated flat plate photovoltaic thermal collector	-
f	friction factor	-
F_R	heat removal factor	-
F_r	Froude number	-
$F`$	collector efficiency factor	-
F	fin efficiency	%
G	mass flux	kg/m^2 s
h	enthalpy	J/kg
$h_{wf,sp}$	single phase heat transfer coefficient	W/m^2K
$h_{wf,mp}$	multi-phase heat transfer coefficient	W/m^2K
h_{fg}	heat of vaporization	J/kg
ORC	organic Rankine Cycle	-
I_s	solar Insulation	W/m^2
k	thermal conductivity	W/m-K
L	length	m
$\dot{m}$	mass flow rate	kg/s
N	dimensionless parameter	-
Nu	Nusselt number	-
P	pressure	MPa
Pr	Prandtl number	-
P.R	pressure ratio	-
PF	packing factor	-
$\dot{Q}$	heat	kW
Re	Reynolds number	-
T	temperature	K
Th	thickness	m
U	heat loss coefficient	W/m^2K
$\dot{V}$	volumetric flow rate	m^3/h
VFR	volume flow ratio	-
w	wind speed	m/s
W	tube spacing	m
$\dot{W}$	work	W
x	vapor quality	-

Subscripts

abs	absorber plate
$abs-g$	absorber to glazing
$g-amb$	glazing to ambient
amb	ambient
bp	boiling point
$conv$	convection
$coll$	solar collector
$crit$	critical
$cond$	condensation
$coll-out$	solar collector outlet
$evap$	evaporation
exp	expander
$exp-out$	expander outlet
g	top glazing
i	isentropic
in	inlet
ins	insulation
l	liquid
$mech$	mechanical
out	outlet
r	reference
rad	radiation
$rank$	rankine
t	tube
T	total
Th	thermal
u	useful
vap	vapor
wf	working fluid

Greek symbols

ϕ	heat flux	W/m^2
ρ	density	kg/m^3
β	PV cell temperature coefficient	$^{\circ}C^{-1}$
$\tau\alpha$	Transmission –absorbance product	-
τ	transmittance	-
η	efficiency	%
σ_{stf}	Stefan-Boltzmann constant	W/m^2K^4
ε	emissivity	-
ν	specific volume	m^3/kg
μ	dynamic viscosity	kg/m s
ψ_{nb}	nucleate boiling factor	-
ψ_{cb}	convective boiling factor	-

Abstract

Heat produced in solar thermal collectors is of low grade which can not be effectively recovered using conventional Rankine cycle systems. Organic Rankine cycle (ORC) is a suitable candidate for low grade heat energy resources. ORC exploits organic fluids operating the cycle at low temperatures. A detailed model of a saturated solar ORC system, using evacuated flat plate photovoltaic thermal collector as a direct vapor generator, is presented in this work. Simulation study is performed for five working fluids to investigate the performance of the system under different pressure ratios and 3 different solar collector configurations (Simple flat plate collector (FPC), Flat plate photovoltaic-thermal (FPV-T) collector, Evacuated flat plate photovoltaic-thermal (EFPV-T) collector). Simulation results revealed that Rankine cycle efficiency and system's thermal efficiency increases when pressure ratio of the cycle is increased while collector thermal efficiency was decreasing with increasing pressure ratio. Results for the 3 collector configurations showed a drop in system performance in case of FPV-T collector configuration while it significantly enhanced in EFPV-T collector configuration. In EFPV-T collector configuration, fluid R600 obtained a maximum net work output and Rankine cycle efficiency of 556.4W and 12.44% respectively. Simulation results for system overall performance revealed that fluid R245fa exhibited the maximum system overall power output of 76.81 W/m^2 and overall electrical efficiency of 8.24%, followed by R601 with system overall power output of 75.97 W/m^2 and overall electrical efficiency of 8.13%,in case of EFPV-T collector configuration at 3.5 pressure ratio. However, high global warming potential of R245fa and high flammability of R601 makes it less attractive.

Keywords: combined photovoltaic-thermal; evacuated flat plate collector; saturated organic Rankine cycle; mathematical modeling; performance analysis.

Chapter 1

Introduction

1.1 Solar Energy

Solar energy is the most vastly available source of renewable energy because the sun never gets exhausted. Even the life on earth wouldn't exist if there was no sun. Sunlight is the key source of energy for almost all life present on earth. The solar energy that is received outside the atmosphere of the earth is 1.366 kW/m^2 and it is called solar constant[1]. Sunlight intensity on surface of earth is not constant but variable because when sunlight enters the earth's atmosphere it gets reflected back to space absorbed and scattered due to presence of clouds, air molecules, dust and water vapor in the atmosphere. It is critical to define a common term known as Air mass (AM)[1];

- **Air mass**

The measure of path length that the solar radiation covers through the earth's atmosphere is called Air mass.

$$AM = {}^{1}/_{\cos z} \tag{1.1}$$

where z represents the zenith angle, between a line drawn perpendicular to surface of earth and line intersecting the sun.

AM0: When the spectrum of sun is outside earth's atmosphere. This value is used for PV modules testing for space applications.

AM1: It describes the case when zenith angle is 0˚; means the sun is directly overhead.

AM1.5: When PV modules are used for terrestrial applications then AM1.5 solar spectrum is commonly used. Zenith angle is 48.2˚ in this case.

- **Solar Insolation or Irradiation and Irradiance**

Incoming solar energy that strikes a unit surface area over some time period is called solar insolation or irradiation. It is expressed in units of kWh/m^2. While the measure of

solar energy per unit area is known as solar irradiance and is expressed in units of W/m^2. Solar irradiance represents the instantaneous value.

As mentioned earlier, when solar radiation travels through earth's atmosphere it is scattered, reflected back to space, and absorbed, so the total amount of solar radiation received on the surface of earth can be divided into two types as follows[1], [2]:

- **Direct radiation**

Direct radiation is that part of solar radiation that reaches the surface of earth directly without any alteration in its direction. It is also known as beam radiation.

- **Diffuse radiation**

Diffuse radiation is that part of solar radiation that reaches the surface of earth after being scattered in the atmosphere.

When the sky is clear and the sun is directly overhead (AM1), there is still 10% diffused radiation component out of the total radiations reaching the surface of earth. With increasing AM value or when there are clouds, the percentage of the diffuse radiations also increases.

- **Global radiation**

The sum of diffused and direct radiation components is called global radiation.

1.2 Solar energy utilization

Different solar energy technologies have been extensively researched, and tested to harvest the free and vastly available solar energy. Solar energy systems are mostly utilized in residential areas and industries for the purpose of electricity production or for domestic water or space heating through solar thermal power plants, solar collectors and photovoltaic devices[3].

1.2.1 Solar thermal collectors

A solar thermal collector collects the incoming solar radiations that are absorbed by the fluid flowing in the collector tubes or available cavities, depending on the collector design[4]. Mostly such collectors are used for water heating.

- **Solar thermal collectors types**

Different types of solar thermal collectors are available in the market today. In general, all these different types follow the same basic principle. The most common types of collectors are presented in Table 1[5];

Table 1 Different types of solar thermal collectors

S. No	Solar thermal collector type	Collector Absorber	Concentration ratio (CR)	Temperature range ˚C
1	Flat-plate solar thermal collector	Flat	1	30 to 80
2	Evacuated-tube collector	Flat	1	50 to 200
3	Parabolic-trough collector	Tube-shaped	15-45	60 to 300
4	Paraboloidal/dish concentrators	Point	100-1000	100 to 500
5	Central receiver	Point	100-1500	150 to 2000

- **Flat-plate solar thermal collector**

As the name indicates, flat plate collector (FPC) has a flat type absorber that collects the solar radiations and is transferred to the working fluid flowing beneath in form of thermal energy. It also consists of a top cover/glazing and insulation at the edges and back to decrease the thermal losses. To enhance the absorptivity of the absorber, it is coated with a special material and is made of a high thermally conductive metal.

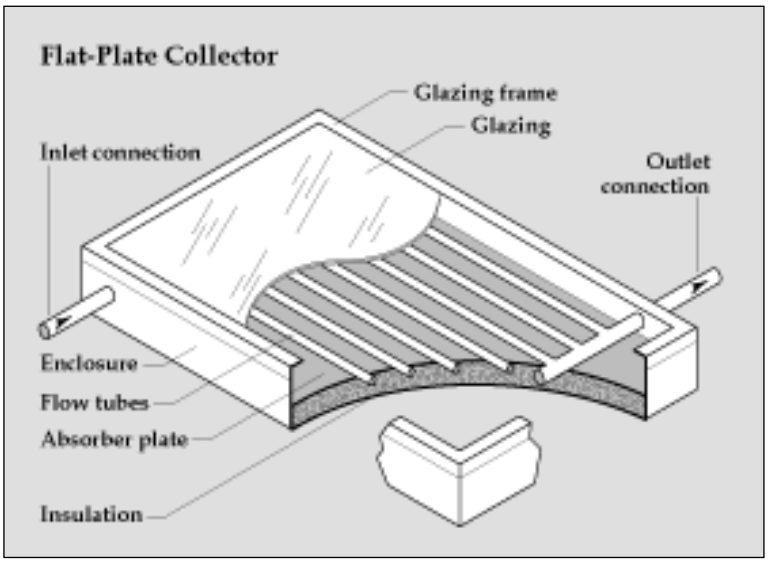

Figure 1 Flat-plate solar thermal collector [6]

- **Evacuated tube collector**

This type of solar thermal collector consists of evacuated tubes and working fluid tubes run inside these tubes. Evacuated tube is the main component in this type of solar collector, which consists of outer glass tube, a selective coated absorber tube and inner copper sheet/fin that has attached tubes for working fluid. The higher efficiency of such collectors is due to low thermal losses, which is accomplished by creating a vacuum between the absorber tube and outer glass tube[7].

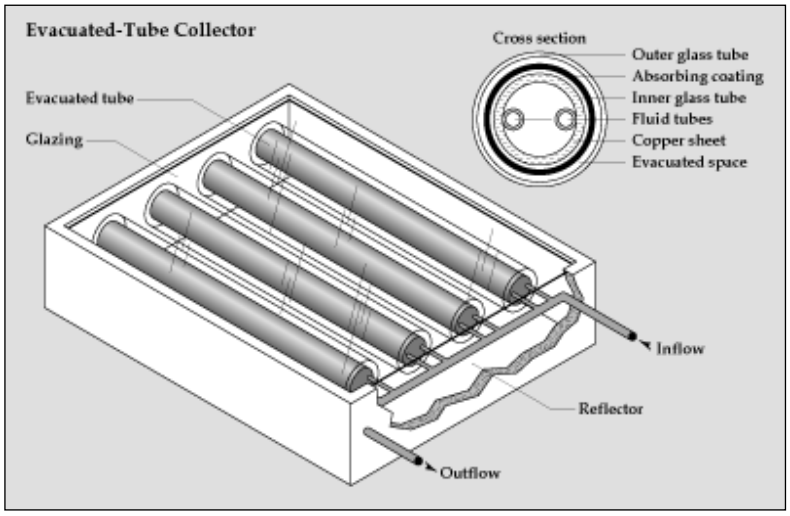

Figure 2 Evacuated-tube solar thermal collector[8]

- **Parabolic trough collectors**

It's a type of concentrating thermal collector that uses a highly polished or reflective surface to collect and concentrate incoming solar radiations on to a tube that contains flowing working fluid. The reflectors are parabolic shaped. Parabolic trough collectors can operate at high temperatures of 60 to 300 ˚C and concentration ratio (CR) ranges from 15-45[5]. For steam production in solar thermal power plants these type of collectors are mostly used.

- **Paraboloidal concentrators**

It's a type of point focus concentrating thermal collector that makes use of a parabolic dish to collect and concentrate solar radiations onto a single point. The parabolic dish is

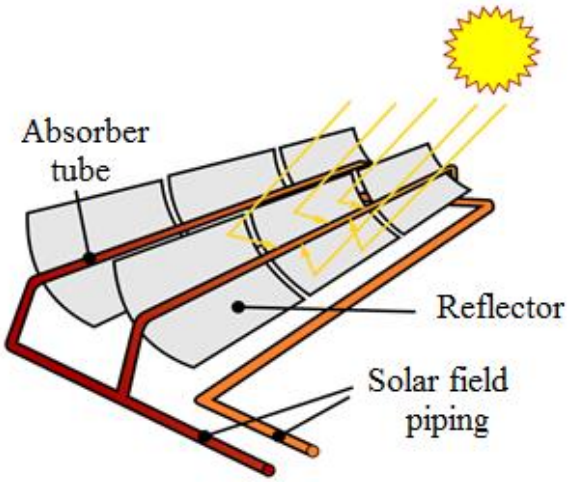

Figure 3 Parabolic-trough collectors [9]

radiations the collector's absorber is positioned[2]. It's a high power solar collector that can achieve temperatures upto 500 ˚C with high concentration ratios of 100-1000[10].

Figure 4 Paraboloidal concentrator or point focus solar thermal collector[11]

- **Central receiver**

This type of solar thermal system comprises of a large field of sun tracking mirrors on the ground that reflect and concentrate the incoming solar radiations at the very top of a tower where receiver or absorber is located. Central receivers are high concentration and

high energy solar collectors and are suitable to produce thermal electric power. Temperatures as high as 1500˚C or even higher can be achieved[10][2].

Figure 5 Central reciever or solar tower [11]

- **Evacuated flat-plate collectors**

Evacuated flat-plate solar thermal collectors combines the technologies of both evacuated tube collectors and FPCs [12]. In this type of solar thermal collectors the air between the absorber-plate and glazing is pumped out to nullify the convective heat transfer losses from the absorber-plate top and only radiation heat transfer occurs between absorber-plate and top glazing[12]. It results in higher heat gain in collector and consequently higher efficiency[13]. Due to vacuum between top glazing and absorber plate, a tight seal is required between glazing and the metal frame. Evacuated flat plate collectors are expensive to manufacture and require sophisticated technology as compare to simple flat plate collectors.

1.2.2 Photovoltaic systems

Photovoltaic (PV) devices convert light energy into electrical energy using semiconductor materials that display photovoltaic effect. Edmond Becquerel was the first in 1839 to discover the photovoltaic effect[14]. The 1st solar cell was developed by Gerald Pearson, Calvin Fuller, and Daryl Chapin that was able to convert enough of solar energy into output power to run electrical equipment, at Bell Lab US[15]. The most widely researched and mature photovoltaic technology is silicon based[16]. Following are the 3 main types of photovoltaic cell technologies that are most commonly available in the market;

- **Monocrystalline cells**

Monocrystalline cells are made out of monocrystalline silicon, which is the most pure form of silicon. In its production process, a cylindrical ingot is created by separating a seed crystal from a bulk of molten silicon. This ingot is of a single, continuous, crystal-lattice structure. Thin wafers are obtained by mechanically slicing the crystal. In the end, required p-n junctiuon is produced by polishing and doping the thin wafers[17]. The manufacturing process is very slow and expensive that is why these are more expensive as compare to polycrystalline or thin films types but is highly efficient.

- **Polycrystalline cells**

Polycrystalline cells' efficiency is less than monocrystalline cells but these are also less expensive because the manufacturing process is less critical and less laborious[17]. Polycrystalline cells are not single crystal silicon but contain many small grains of crystals. The presence of grain boundaries reduces the cell performance by obstructing carrier flows and permitting extra energy levels in forbidden gap. Polycrystalline cells can be made from molten silicon by casting a cube shaped ingot and then sliced into wafers just like monocrystalline cells.

- **Thin film cells**

Amorphous silicon is a type of thin film photovoltaic cells. To produce amorphous cells, thin layers of silicon are deposited on glass substrate. Silicon being used in its production is very less as compare to that in producing crystalline cells[17]. These are very cheap to produce because of the less energy intensive manufacturing process and less use of raw material. However, the efficiency is greatly reduced because the silicon atoms are not arranged in order as compare to crystalline cells.

1.2.3 Photovoltaic-Thermal systems

Photovoltaic-thermal (PV-T) systems are also called hybrid solar thermal collectors or solar cogenerations systems. Electricity and heat is generated at the same time utilizing the solar energy in PV-T collectors [18]. In such solar cogeneration systems, PV cells are laminated or bonded to the absorber plate. The PV cells produce electricity and the collector produce thermal energy. PV-T systems solve the major space consumption

issue, if PV system and solar collectors are used separately[19]. The combined output of PV-T system is more as compare to using PV system alone.

PV-T systems are classified into 4 categories, in terms of heat removal medium. The heat removal mediums are as follows;

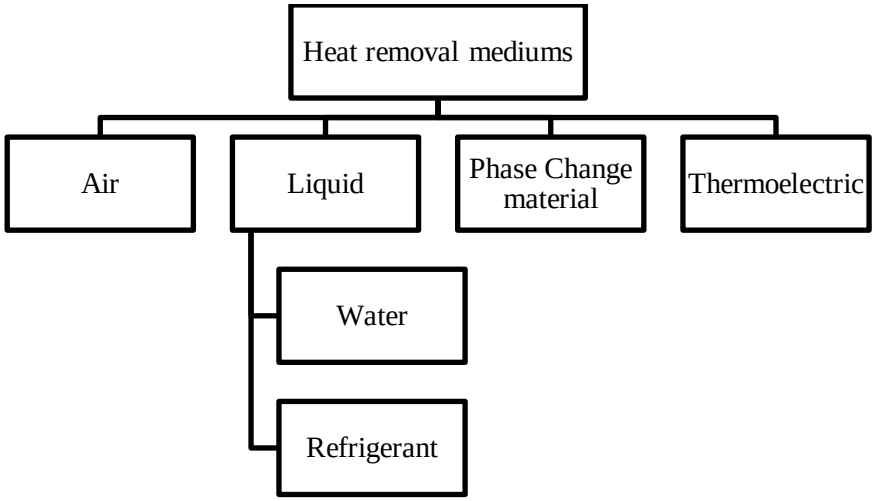

Figure 6 Different types of heat removal mediums

In terms of system's configuration, PV-T systems are classified into following 3 categories;

- Flat plate PV-T collectors

One type of hybrid solar thermal collector is called "Flat plat photovoltaic-thermal (FPV-T) collector". In FPV-T collector, photovoltaic module or cells are bonded over the absorber plate of the collector.

- Concentrated PV-T collectors

In concentrated PVs, the solar radiations are focused (concentrated) using lenses or mirrors, onto a highly efficient and small, multi-junction cell to generate electricity[20]. Due to high concentration of solar radiations the solar cells operate at very high temperatures and could adversely affect the cell's electrical efficiency and cause degradation[20]. To remove this heat and lower the PV cells temperature, a cooling unit can be attached to the back surface of the concentrated PV module creating a concentrated PV-T collector.

- Building integrated PV-T collectors

In building integrated PV-T collectors, the PV-T system is incorporated into building envelop such as facades, windows or roof to produce electricity and thermal energy simultaneously.

1.2.4 Direct solar vapor generation

When a liquid working fluid changes its phase and evaporates completely in the solar collector tubes then it is called a direct vapor generation solar collector, because vapors are generated directly in the solar collector tubes without the need of any external heat exchanger or heat source apart from solar radiations[21], [22].

One of the main uses of the generated vapor is in Rankine vapor cycle for electricity production. Rankine vapor cycle process is most widely implemented in thermal power plants such as nuclear reactors, or natural gas or coal fired power plant. In thermal power plants heat energy is converted into electrical energy. In Rankine cycle system, fuel is burnt to generate heat that vaporizes water in the boiler tubes and then the steam expands through a turbine generating useful work. Scottish engineer William J.M. Rankine was the first to develop this process in 1859. Working fluid is continuously reused in the closed cycle. Hence, fluid should be stable and not change its chemical properties under continuous phase changing. Water is the most practical working fluid for this cycle.

Water with high heat of vaporization requires high temperatures to convert it into steam in the boiler. Therefore, Rankine cycle can't efficiently utilize low temperatures[23]. When heat of low grade is available, orgainc Rankine cycle (ORC) is implemented to generate electricity effectively.

1.2.5 Organic Rankine Cycle

Organic Rakine cycle (ORC) follows the similar basic working principle as that of simple Rankine cycle, aside from utilizing different working fluid. ORC can efficiently utilize low temperatures by incorporating organic fluids as working fluids. Organic fluids' boiling point is much lower as compare to water hence such fluids will evaporate faster and at lower temperatures[24].

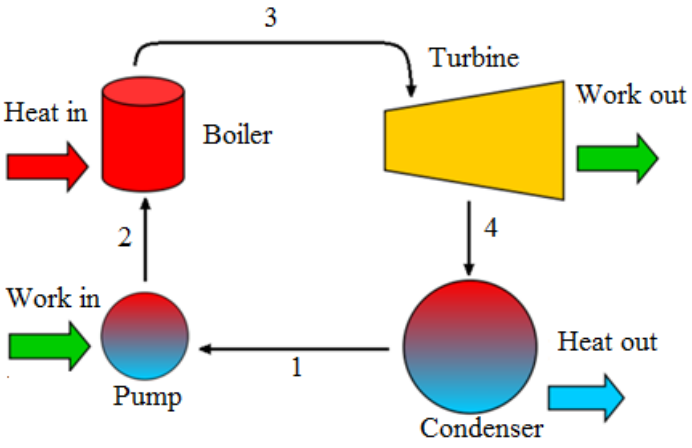

Figure 7 Schematic for Rankine cycle

Presented in Figure 7 are the 4 most basic steps involved in ORC process. Following are the main components of the ORC;

- Pump: Initially working fluid is at cycle's lower pressure which is compressed to higher pressure, in pump. It consumes power (work input) and the process is shown in the Figure 7 as step 1 - step 2.
- Boiler: Now that the working fluid is pressurized to the boiler pressure it enters the boiler tubes or cavity where it gains thermal energy. The working fluid is completely evaporated in the boiler from liquid to vapor phase (step 2 - step 3).
- Turbine/Expander: The evaporated working fluid enters the turbine/expander where it expands from high pressure to lower condenser pressure, generating useful work (step 3 - step 4).
- Condenser: Vapor at the outlet of the turbine enters the condenser where it changes its phase from vapor to liquid (step 4 - step 1). Heat is rejected in the condenser.

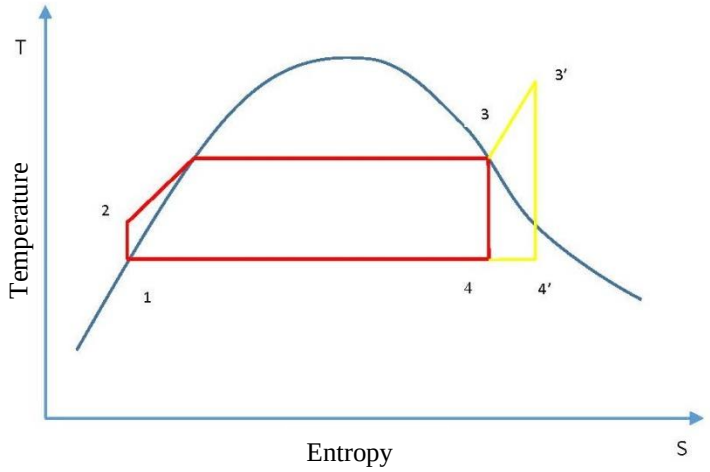

Figure 8 Temperature vs entropy (T-S) diagram for Rankine cycle[11]

Figure 8 presents the ideal temperature-entropy relationship for the Rankine cycle presented in Figure 7. It can be observed that working fluid is compressed to higher pressure at constant entropy. Pressure remains constant in the boiler, from point 2 to point 3. Point 3 is saturated vapor point. To increase the work output and to minimize moisture content at the outlet end of turbine, working fluid is often superheated (point 3'). Vapor then expands through the turbine at constant entropy. Vapor is condensed to saturated liquid at constant pressure.

1.2.6 Solar Organic Rankine Cycle

In solar ORC, the input heat required to vaporize the working fluid is delivered through solar-thermal collectors utilizing the solar energy. Solar collector can either be used as direct vapor generator (to evaporate the working fluid) or it can be used to heat up high heat capacity thermal oil that will pass through another heat exchanger (evaporator) where heat is transferred to the Rankine cycle working fluid, as shown in Figure 9.

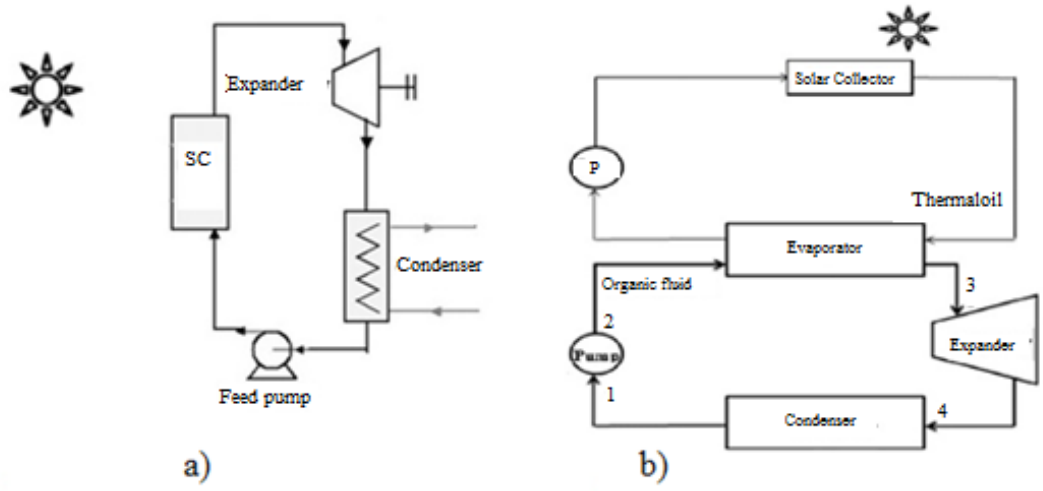

Figure 9 Solar ORC (a) Direct vapor generation (b) Separate evaporator [11]

1.3 Study Objectives

The performance of the saturated solar ORC system for three collector configurations are compared using seven different working fluids and under different pressure ratio points. The main objectives of this study are:

- To compare and investigate the performance of solar collector (evaporator) for simple flat plate collector (FPC), flat plate photovoltaic-thermal collector (FPV-T) and evacuated flat plate PVT (EFPV-T) collector configurations.
- To compare and investigate the performance of saturated solar ORC system for simple FPC, FPV-T and EFPV-T collector configurations.
- To examine the solar collector's absorber temperature and its effect on the PV module's performance.
- Investigate the system overall electrical output and overall electrical efficiency for FPV-T and EFPV-T collector configurations.
- To select a suitable working fluid in terms of its overall performance.

A detailed mathematical model has been worked out for a low temperature saturated solar ORC system using solar thermal collectors as direct vapor generator (evaporator). The model is investigated for three different types of solar thermal collector configurations. The three collector configurations are described below:

1. Simple flat plate collector (FPC): A conventional flat plate solar thermal collector that is commonly available in the market.
2. Flat plate photovoltaic-thermal collector (FPV-T): In this case, a PV module is covering the top surface of the collector's absorber plate.
3. Evacuated flat plate photovoltaic-thermal collector (EFPV-T): The air between the collector's top glazing and PV-absorber plate layer is pumped out that will diminish the natural convective heat transfer between top glazing and PV-absorber plate layer hence decreasing the top heat loss coefficient and increasing the thermal efficiency of the collector.

1.4 Limitations of Study

This work comprises of mathematical modeling and simulation observations. The model for saturated solar ORC has the following simulation constraints:

- Working fluid exits the collector and condenser as saturated vapor and saturated liquid, respectively. No superheating at the collector outlet and subcooling at the condenser outlet were achieved, to avoid the increase in cycle irreversibility[25].
- Expander's isentropic efficiency, expander mechanical efficiency and isentropic efficiency of pump are 70%, 95% and 80% respectfully and remain constant [26], [27].
- Maximum evaporating pressure in flat plate solar collector is 1.5MPa and minimum allowable condenser pressure is 0.005MPa[27]–[29].
- Simulations are performed at constant condensing temperature of 37 ˚C.
- PV is completely covering the top surface of the absorber plate. A perfect bond is assumed between absorber plate and PV. The PV cells and absorber plate temperatures are considered to be equal[25].

1.5 Thesis outline

The detailed sections of this study are summarized below.

Chapter 1: Introduction to solar energy, basic definitions and different systems that utilize solar energy to generate heat or electricity have been discussed in this chapter. Main objectives and limitations of the thesis are also included at the chapter's end.

Chapter 2: This chapter will summarize the research work done on flat plate solar thermal collectors, evacuated flat plate solar thermal collectors, FPV-T collectors and solar ORC. This section will help us better understand the performance characteristics of flat plat solar thermal collectors and solar ORC. Furthermore, limitations of this study and research methodology have also been explained in this section.

Chapter 3: In this chapter, complete mathematical model for the proposed solar ORC system will be developed and the Matlab simulation procedure has been explained. It will also provide initial analysis, performed for solar thermal collector using the developed mathematical model, for validation purpose. Working fluids selection procedure has also been explained.

Chapter 4: This chapter will sum up the final simulation results. Detailed performance analysis of three solar thermal collector configurations and solar ORC will be presented and comparatively analyzed.

Chapter 5: This chapter will be comprised of conclusion, recommendations and the work which will be carried out in the future.

Summary

In this chapter a brief introduction to solar energy and its different uses have been discussed. Solar energy products have found its path into the market for commercial and residential use, in past few decades. Solar energy has been utilized for space heating, hot water in winter, generating steam/vapor for electricity production through Rankine cycle etc. There are five most commonly available solar thermal collectors. Concentration ratio of these collectors ranges from 1 to 1500 and temperature ranges from 30˚C to 2000 ˚C. Organic Rankine cycle is another technology that can utilize solar thermal energy and generate electricity. In the end of the chapter, main objectives and limitations of current study has been included.

References

[1] D. Y. Goswami, *Principles of solar engineering*. CRC Press, 2015.

[2] F. Daniels, “Solar energy,” *Science (80-.).*, vol. 109, no. 2821, pp. 51–57, 1949.

[3] R. Agrawal, K. Kushwaha, and G. Patel, “A Review of Renewable Energy Resources: Current Status and Their Enabling Technology,” *Int. J. Pollut. Noise Control*, vol. 1, no. 2, pp. 36–44, 2016.

[4] S. A. Kalogirou, “Solar thermal collectors and applications,” *Prog. energy Combust. Sci.*, vol. 30, no. 3, pp. 231–295, 2004.

[5] S. Kalogirou, “The potential of solar industrial process heat applications,” *Appl. Energy*, vol. 76, no. 4, pp. 337–361, 2003.

[6] “File:Flat plate glazed collector.gif - Wikimedia Commons.” [Online]. Available: https://commons.wikimedia.org/wiki/File:Flat_plate_glazed_collector.gif. [Accessed: 11-Dec-2019].

[7] M. A. Sabiha, R. Saidur, S. Mekhilef, and O. Mahian, “Progress and latest developments of evacuated tube solar collectors,” vol. 51, pp. 1038–1054, 2015.

[8] “File:Evacuated tube collector.gif - Wikimedia Commons.” [Online]. Available: https://commons.wikimedia.org/wiki/File:Evacuated_tube_collector.gif. [Accessed: 11-Dec-2019].

[9] “File:Parabolic trough.svg - Wikimedia Commons.” [Online]. Available: https://commons.wikimedia.org/wiki/File:Parabolic_trough.svg. [Accessed: 11-Dec-2019].

[10] S. Mekhilef, R. Saidur, and A. Safari, “A review on solar energy use in industries,” *Renew. Sustain. Energy Rev.*, vol. 15, no. 4, pp. 1777–1790, 2011.

[11] “Category:Solar Stirling engines - Wikimedia Commons.” [Online]. Available: https://commons.wikimedia.org/wiki/Category:Solar_Stirling_engines. [Accessed: 11-Dec-2019].

[12] P. Henshall, R. Moss, F. Arya, P. Eames, S. Shire, and T. Hyde, “An evacuated enclosure design for solar thermal energy applications,” *Gd. Renew. Energy 2014*, no. 1, pp. 2–5, 2014.

[13] R. W. Moss, P. Henshall, F. Arya, G. S. F. Shire, T. Hyde, and P. C. Eames, “Performance and operational effectiveness of evacuated flat plate solar collectors compared with conventional thermal, PVT and PV panels,” *Appl. Energy*, vol. 216, no. August 2017, pp. 588–601, 2018.

[14] G. Boyle, “Renewable energy,” *Renew. Energy, by Ed. by Godfrey Boyle, pp. 456. Oxford Univ. Press. May 2004. ISBN-10 0199261784. ISBN-13 9780199261789*, p. 456, 2004.

[15] K. A. Tsokos, *Physics for the IB Diploma Full Colour*. Cambridge University Press, 2010.

[16] “Common Types of Solar Cells - What are Better Silicon, Monocrystalline, or Polycrystalline Solar Cells?” [Online]. Available: http://www.altenergy.org/renewables/solar/common-types-of-solar-cells.html. [Accessed: 27-Nov-2019].

[17] S. Peake, *Renewable energy-power for a sustainable future.*, no. Ed. 4. Oxford university press, 2018.

[18] H. A. Zondag, “Thermal and Electrical Yield of a Combi-Panel,” *Proc. ISES Sol. World Congr.*, vol. III, pp. 96–101, 1999.

[19] H. A. Zondag, D. W. D. E. Vries, W. G. J. V. A. N. Helden, R. J. C. V. A. N. Zolingen, and A. A. V. A. N. Steenhoven, “THE THERMAL AND ELECTRICAL YIELD OF A PV-THERMAL COLLECTOR,” vol. 72, no. 2, pp. 113–128, 2002.

[20] G. Kosmadakis, D. Manolakos, and G. Papadakis, “Simulation and economic analysis of a CPV/thermal system coupled with an organic Rankine cycle for increased power generation,” *Sol. Energy*, vol. 85, no. 2, pp. 308–324, 2011.

[21] M. Marion, I. Voicu, and A.-L. Tiffonnet, “Study and optimization of a solar subcritical organic Rankine cycle,” *Renew. Energy*, vol. 48, pp. 100–109, 2012.

[22] A. M. Delgado-Torres and L. García-Rodríguez, “Analysis and optimization of the low-temperature solar organic Rankine cycle (ORC),” *Energy Convers. Manag.*, vol. 51, no. 12, pp. 2846–2856, 2010.

[23] H. Chen, D. Y. Goswami, and E. K. Stefanakos, “A review of thermodynamic cycles and working fluids for the conversion of low-grade heat,” *Renew. Sustain. energy Rev.*, vol. 14, no. 9, pp. 3059–3067, 2010.

[24] J. P. Roy and A. Misra, “Parametric optimization and performance analysis of a regenerative Organic Rankine Cycle using R-123 for waste heat recovery,” *Energy*, vol. 39, no. 1, pp. 227–235, 2012.

[25] H. Zhai, L. Shi, and Q. An, “In fl uence of working fl uid properties on system performance and screen evaluation indicators for geothermal ORC (organic Rankine cycle) system,” *Energy*, 2014.

[26] B. F. Tchanche, G. Papadakis, G. Lambrinos, and A. Frangoudakis, “Fluid selection for a low-temperature solar organic Rankine cycle,” *Appl. Therm. Eng.*, vol. 29, no. 11–12, pp. 2468–2476, 2009.

[27] X. D. Wang, L. Zhao, J. L. Wang, W. Z. Zhang, X. Z. Zhao, and W. Wu, “Performance evaluation of a low-temperature solar Rankine cycle system utilizing R245fa,” *Sol. Energy*, vol. 84, no. 3, pp. 353–364, 2010.

[28] J. Bao and L. Zhao, “A review of working fl uid and expander selections for organic Rankine cycle,” *Renew. Sustain. Energy Rev.*, vol. 24, pp. 325–342, 2013.

[29] U. Helvaci and Z. Khan, “Thermodynamic modelling and analysis of a solar organic Rankine cycle employing thermofluids,” *Energy Convers. Manag.*, vol. 138, Feb. 2017.

Chapter 2

Literature review

2.1 Flat Plate Collectors

Over the past few decades, extensive research has been conducted on the modeling, and experimental and theoretical performance analysis of various types of solar thermal collectors. This section focuses on the researches that have been done on the flat plate solar thermal collectors' mathematical modeling and performance prediction.

The very first model and performance evaluation of flat plate collector was presented by [1], [2]. The heat capacities of different components of collector are not included in this model, and it is very convenient to use [3], [4]. The useful heat gain for solar flat plate collectors can be represented as follows[4];

$$Q_u = A_c F_r [I_s(\tau\alpha) - U_T(T_{in} - T_{amb})] \tag{2.1}$$

Where A_c and F_r represent the area of collector and heat removal factor. T_{amb} and T_{in} are the fluid's ambient and inlet temperature, respectively. I_s, U_T and $\tau\alpha$, respectively represent the solar irradiance, collector overall heat loss coefficient and transmission-absorption constant. Heat removal factor is evaluated using the following formula [4];

$$F_r = \frac{\dot{m}_{wf} C_p}{A_c U_T}\left[1 - \exp\left(\frac{-A_c U_T F`}{\dot{m}_{wf} C_p}\right)\right] \tag{2.2}$$

In above Equation (2.2), $\dot{m}_{wf}$ represents the working fluid's mass flow rate in tubes and $F`$ represents the collector efficiency factor.

$$F` = \frac{(U_T)^{-1}}{W[U_T(D_{out}+(W-D_{out})F)]^{-1}+(C_b)^{-1}+\left(\pi D_{in} h_{wf}\right)^{-1}} \tag{2.3}$$

where D_{out} and D_{in} are the tube's outer and inner diameter, respectively. W is the spacing between tubes and $C_b$is the bond conductance which is very large ($(C_b)^{-1} = 0$). F denotes the fin efficiency and can be represented as;

$$F = \frac{\tanh\left[m\left(W - {D_{out}}/{2}\right)\right]}{m\left(W - {D_{out}}/{2}\right)} \tag{2.4}$$

where the coefficient m for simple flat plate collectors is determined by Equation (2.5);

$$m = \sqrt{\frac{U_T}{k_{abs} th_{abs}}} \tag{2.5}$$

Overall heat loss coefficient of the collector U_T is the addition of "collector's top heat loss coefficient U_{top} and back heat loss coefficient U_{Back}". There are 2 conventional approaches to determine U_{top}; thermal network[4] or a generalized formula[3].

A transient mathematical model for FPC with liquid as a working fluid was established[5]. Energy conservation equations were developed for the fluid flowing in the collector tube and using implicit finite difference iterative method the temperature of fluid and tube wall were determined. Thermal performance study of a transpired unglazed solar collector was conducted[6]. Using energy balance equations, a mathematical model was established and constructed for 3 main components of the system; absorber, working fluid (air) and back plate. 7 different parameters were investigated for the performance study of the unglazed transpired solar thermal collector. The main performance parameters were thermal efficiency and heat exchange effectiveness. It was observed that working fluid flow rate, collector pitch and solar absorptivity were the key factors influencing the collector's performance parameters[6].

- **Evacuated Flat Plate Solar Thermal Collectors**

Solar FPCs experience thermal losses that decrease its thermal efficiency. Thermal energy is lost to the environment from collectors' top, back and edges. Thermal energy loss from the collector is mostly from the top while thermal loss through the collector's edges is considered negligible. As it can be observed from Figure 10 that top heat loss occurs due to convection, radiation and reflection. There are two types of convection losses; Forced convection from collector's top glazing to ambient and natural convection between absorber plate and top glazing.

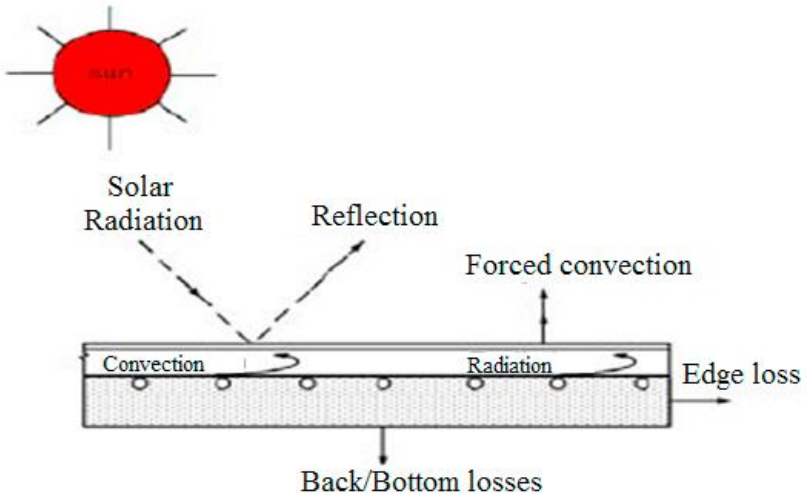

Figure 10 Flat plate collector's thermal losses

Thermal losses from the collector's top can be decreased by creating a vacuum between absorber plate and top glass cover that will diminish the natural convective heat transfer. Such solar collectors are known as evacuated flat plate solar thermal collectors and have been numerically and experimentally investigated by a number of researchers.

For the application of process steam production in industries, [7] developed an evacuated flat plate collector. Selective coated copper absorber with very low emissivity was used to lower the radiation losses. The collector was not completely evacuated but a partial evacuation down to 1000 Pa was obtained (no natural convection occurs but gas heat conduction is still active)[7]. To lower the gas thermal conduction, air was replaced by chemically inert gas. The molar mass and collision cross-section of this gas was high and number of degrees of freedom was low. The developed evacuated collector observed high thermal efficiencies at high temperatures[7]. Theoretical study of a flat plate collector with vacuum glazing under different configurations was conducted by [8]. In this type of vacuum collector the air between top glass cover and absorber plate is not evacuated but rather a new design glazing is used, which is made of two sheets of glass bonded together along the edges and the space between the sheets is evacuated. They modeled the collector using energy balance equations and design tool KOLEKTOR 2.0. It was reported that the vacuum glazing flat plate collector revealed higher efficiency than most of the evacuated tube collectors[8]. A flat plate collector with evacuated enclosure of very low pressure 0.1 Pa is designed and investigated by [9]. At such low

pressure, both natural convection and gas conduction between absorber plate and top collector glazing is completely suppressed. To support the glass cover under atmospheric pressure and to make sure the performance of sealing material in the long term, array of support pillars are introduced in the collector design. Collector's top heat loss coefficient was significantly reduced and higher thermal efficiency for vacuum FPC was reported[9].

- **Flat Plate Photovoltaic-Thermal Collector**

Flat plate photovoltaic-thermal (FPV-T) collector or hybrid PV-T collectors are systems that convert solar radiations into thermal energy and electricity at the same time [10], [11]. In FPV-T collectors the photovoltaic module or cells are bonded/laminated over the top surface of the collector's absorber plate. Photovoltaic cells generate electrical energy and working fluid flowing in the tubes of the collector heats up and deliver thermal energy.

A substantial amount of research has been conducted on hybrid PV-T systems. Thermal and electrical efficiencies of PV-T collector for three different types of collector designs was experimentally investigated [12]. Experimental results revealed that PV-T solar collector with spiral flow type absorber obtained higher PV electrical and thermal efficiency of 13.8% and 54.6% respectively. Another detailed mathematical model of a glazed PV-T water collector was established and it was found that the overall efficiency of PV-T collector is higher as compare to simple PV module[13]. PV electricity production was found to be lower in PV-T collector but, at the same time, thermal energy is also produced in PV-T collector [13]. Another mathematical modeling and experimental study of different PV-T collector designs was performed by [14]. PV-T collector with PV cells bonded on sheet and tube absorber plate is recommended by the authors[14]. It was also reported that hybrid PV-T collector gives more output per unit area than a conventional thermal collector and PV system placed together[14].

2.2 Solar Organic Rankine Cycle

As described in previous chapter that in solar ORC the input heat required to evaporate the working fluid is delivered through solar thermal collectors utilizing the solar energy.

Extensive research has been conducted on solar ORC systems using solar thermal collectors as evaporators (direct vapor generation) or using an intermediate heat exchanger (evaporator) that will extract heat from high capacity working fluid coming from solar collector array.

A low temperature solar Rankine cycle was designed for reverse osmosis desalination utilizing vacuum tube solar collectors array is established by [15]. HFC-134a was used as working fluid in Rankine cycle and water was used as heat transfer fluid in solar collector. TRNSYS software was used for model simulations and the study reported system efficiency of about 7% [15]. Study of a low cost solar ORC coupled with parabolic trough collectors is conducted by[16]. In the study, the heat transfer fluid was Monoethylene glycol and different ORC working fluids were comparatively analyzed. It was concluded that Solkatherm is the most efficient working fluid but require larger expander size due to higher volume flow rate, on the other hand R245fa was reported to show good efficiency with smaller expander size requirement[16].

Experimental study on the performance evaluation of low temperature solar ORC utilizing solar thermal collectors as direct vapor generators is conducted by [17]. Two types of solar collectors, evacuated tube and flat plate collectors were investigated utilizing R245fa as working fluid. It was found that evacuated tube collectors are more efficient and the ORC system achieved overall generation efficiency of 4.2% as compare to flat plate collectors where system achieved overall generation efficiency of about 3.2%[17]. It was also reported that fluid R245fa is a feasible working fluid for low temperature solar ORC systems[17]. Another study of low temperature solar ORC utilizing solar thermal collector as direct vapor generator is conducted by [18]. Flat plate collector and solar ORC system is mathematically modeled and 24 working fluids are comparatively analyzed under increasing pressure ratios. Working fluid selection guidelines were presented in detail [18].

PV-T collectors have also attracted considerable attention and have been widely investigated, both as separate PV-T system or coupled with ORC. The performance of PV-T ORC system for 27 working fluids, and under different ORC configurations and different types of PV cells was evaluated by [19]. Working fluid n-Butane was found to

be the most suitable candidate and CdS PV cells exhibited the best performance[19]. Simulation study for concentrating PV-T (CPV-T) system combined with ORC was established in[20]. The authors concluded that combined CPV-T ORC showed a higher annual efficiency and net power output as compare to using CPV system alone[20].

Performance of ORC is greatly influenced by the choice of working fluid. There are many working fluids available and several working fluid selection studies have been conducted [21]–[25]. Hydrochlorofluorocarbons (HCFCs) and chlorofluorocarbons (CFCs) have once dominated the refrigerants market but due to their ozone depletion potential (ODP) these fluids have either been completely banned or in the process of phasing out [26]–[28]. Hydrofluorocarbons (HFCs) fluids with zero ODP provide a better alternative to HCFCs and CFCs[29]. HFC-R245fa have been suggested by several researchers as a good candidate for ORC systems [17], [24], [30]. On the other hand Hydrocarbons (HCs) i.e. R290, R600, R600a, R601 present zero ODP, low GWP, low cost and availability[31]. Hydrofluoroolefins (HFOs) i.e. R1234ze(E) and R1234yf are also promising alternatives with very low GWP [29], [32].

2.3 Research Methodology

The research methodology adopted for this study is shown in Figure 11 and it starts from the very initial step of topic selection and literature review. Literature review is divided into two main topics to understand the background of the selected work. Then the proposed Solar ORC coupled with EFPV-T system is modeled under steady state condition. The mathematical model is then coded using MATLAB simulation tool and working fluid's thermo-physical properties are imported from COOLPROP software[33]. Weather data for Islamabad, Pakistan is obtained from Meteonorm database[34]. Simulation results are obtained and different performance parameters are investigated and performance of three different solar thermal collector configurations are comparatively analyzed.

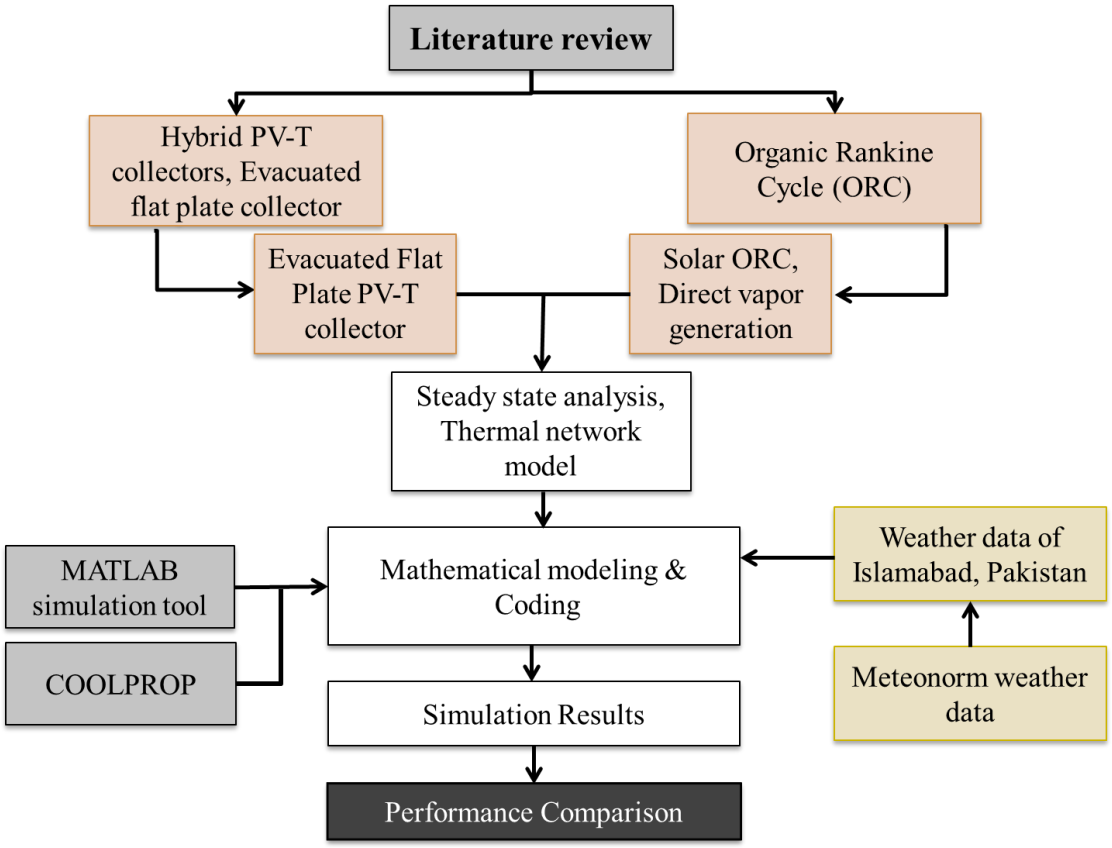

Figure 11 Block Diagram of Research Methodology

Summary

In this chapter, extensive literature review for solar thermal collectors and solar ORC have been presented. A wide range of mathematical and theoretical models for performance analysis of solar thermal collectors were found. The very first model was established for simple FPC type. Evacuated flat plate collectors brought some enhancement in the thermal efficiency over simple flat plate collector by lowering the overall heat loss coefficient of the collector. It was achieved by lowering the air pressure between absorber and glazing or by creating a complete vacuum. Literature review for flat plate photovoltaic-thermal collector revealed that such hybrid collectors generate more combined output as compare to PV system or a simple collector utilized separately. Hybrid collectors have PV cells bonded/laminated over the absorber plate that directly generates electricity. Solar thermal collectors can also be coupled with ORC system to generate electricity, commonly known as solar ORC . In solar ORC, collectors can either be used as a separate heat exchanger or used directly to generate vapor.

References

[1] H. Hottel and A. Whillier, “Evaluation of flat-plate solar collector performance,” in *Trans. Conf. Use of Solar Energy;()*, 1955, vol. 3.

[2] A. Whillier, “Solar Energy Collection and its Utilization for House Heating.” p. 202, 1953.

[3] S. A. Klein, “Calculation of flat-plate collector loss coefficients,” *Sol. Energy*, vol. 17, no. 1, pp. 79–80, 1975.

[4] John A Duffie and W. A. Beckman, *Solar Engineering of Thermal Processes Solar Engineering*. 2013.

[5] W. Zima and P. Dziewa, “Mathematical modelling of heat transfer in liquid flat-plate solar collector tubes,” *Arch. Thermodyn.*, vol. 31, no. 2, pp. 45–62, 2010.

[6] M. A. Leon and S. Kumar, “Mathematical modeling and thermal performance analysis of unglazed transpired solar collectors,” *Sol. Energy*, vol. 81, no. 1, pp. 62–75, 2007.

[7] N. BENZ and T. BEIKIRCHER, “HIGH EFFICIENCY EVACUATED FLAT-PLATE SOLAR COLLECTOR FOR PROCESS STEAM PRODUCTION1Paper presented at the ISES Solar World Congress, Taejon, South Korea, 24–29 August 1997.1,” *Sol. Energy*, vol. 65, no. 2, pp. 111–118, 1999.

[8] V. Shemelin and T. Matuska, “Detailed Modeling of Flat Plate Solar Collector with Vacuum Glazing,” *Int. J. Photoenergy*, vol. 2017, 2017.

[9] P. Henshall, R. Moss, F. Arya, P. Eames, S. Shire, and T. Hyde, “An evacuated enclosure design for solar thermal energy applications,” *Gd. Renew. Energy 2014*, no. 1, pp. 2–5, 2014.

[10] E. C. Kern Jr and M. C. Russell, “Combined photovoltaic and thermal hybrid collector systems,” Massachusetts Inst. of Tech., Lexington (USA). Lincoln Lab., 1978.

[11] A. Makki, S. Omer, and H. Sabir, “Advancements in hybrid photovoltaic systems for enhanced solar cells performance,” *Renew. Sustain. Energy Rev.*, vol. 41, pp. 658–684, 2015.

[12] A. Fudholi, K. Sopian, M. H. Yazdi, M. Hafidz, A. Ibrahim, and H. A. Kazem, “Performance analysis of photovoltaic thermal (PVT) water collectors,” *ENERGY Convers. Manag.*, vol. 78, pp. 641–651, 2014.

[13] F. Leonforte and C. Del Pero, “Modeling and Performance Monitoring of a Photovoltaic – Thermal (PVT) Water Collector,” *Sol. Energy*, vol. 112, pp. 85–99, 2015.

[14] H. A. Zondag, D. W. de Vries, W. G. J. van Helden, R. J. C. van Zolingen, and A. A. van Steenhoven, “The yield of different combined PV-thermal collector designs,” *Sol. Energy*, vol. 74, no. 3, pp. 253–269, 2003.

[15] D. Manolakos, G. Papadakis, E. Sh, and S. Kyritsis, “Design of an autonomous low-temperature solar Rankine cycle system for reverse osmosis desalination,” vol. 183, no. May, pp. 73–80, 2005.

[16] S. Quoilin, M. Orosz, H. Hemond, and V. Lemort, “Performance and design optimization of a low-cost solar organic Rankine cycle for remote power generation,” *Sol. Energy*, vol. 85, no. 5, pp. 955–966, 2011.

[17] X. D. Wang, L. Zhao, J. L. Wang, W. Z. Zhang, X. Z. Zhao, and W. Wu, “Performance evaluation of a low-temperature solar Rankine cycle system utilizing R245fa,” *Sol. Energy*, vol. 84, no. 3, pp. 353–364, 2010.

[18] U. Helvaci and Z. Khan, “Thermodynamic modelling and analysis of a solar organic Rankine cycle employing thermofluids,” *Energy Convers. Manag.*, vol. 138, Feb. 2017.

[19] K. Tourkov and L. Schaefer, “Performance evaluation of a PVT/ORC (photovoltaic thermal/organic Rankine cycle) system with optimization of the ORC and evaluation of several PV (photovoltaic) materials,” *Energy*, vol. 82, pp.

839–849, 2015.

[20] G. Kosmadakis, D. Manolakos, and G. Papadakis, “Simulation and economic analysis of a CPV/thermal system coupled with an organic Rankine cycle for increased power generation,” *Sol. Energy*, vol. 85, no. 2, pp. 308–324, 2011.

[21] J. Bao and L. Zhao, “A review of working fl uid and expander selections for organic Rankine cycle,” *Renew. Sustain. Energy Rev.*, vol. 24, pp. 325–342, 2013.

[22] P. Gang, L. Jing, and J. Jie, “Working Fluid Selection for Low Temperature Solar Thermal Power Generation with Two-stage Collectors and Heat Storage Units.”

[23] X. G. Li, W. J. Zhao, D. D. Lin, and Q. Zhu, “Working fluid selection based on critical temperature and water temperature in organic Rankine cycle,” *Sci. China Technol. Sci.*, vol. 58, no. 1, pp. 138–146, 2014.

[24] J. Kajurek, A. Rusowicz, A. Grzebielec, W. Bujalski, K. Futyma, and Z. Rudowicz, “Selection of refrigerants for a modified organic Rankine cycle,” *Energy*, vol. 168, pp. 1–8, 2019.

[25] Z. Q. Wang, N. J. Zhou, J. Guo, and X. Y. Wang, “Fluid selection and parametric optimization of organic Rankine cycle using low temperature waste heat,” *Energy*, vol. 40, no. 1, pp. 107–115, 2012.

[26] R. L. Powell, “CFC phase-out: Have we met the challenge?,” *J. Fluor. Chem.*, vol. 114, no. 2, pp. 237–250, 2002.

[27] T. Parties, B. Parties, V. Convention, O. Layer, V. Convention, and O. Layer, “Montreal protocol on substances that deplete the Ozone layer final act 1987,” *J. Environ. Law*, vol. 1, no. 1, pp. 128–136, 1989.

[28] K. J. Park, T. Seo, and D. Jung, “Performance of alternative refrigerants for residential air-conditioning applications,” *Appl. Energy*, vol. 84, no. 10, pp. 985–991, 2007.

[29] B. Saleh, “Parametric and working fluid analysis of a combined organic Rankine-

vapor compression refrigeration system activated by low-grade thermal energy," *J. Adv. Res.*, vol. 7, no. 5, pp. 651–660, 2016.

[30] T. Guo, H. Wang, and S. Zhang, "Working fluids of a low-temperature geothermally-powered Rankine cycle for combined power and heat generation system," *Sci. China Technol. Sci.*, vol. 53, no. 11, pp. 3072–3078, 2010.

[31] A. Kabul, Ö. Kizilkan, and A. K. Yakut, "Performance and exergetic analysis of vapor compression refrigeration system with an internal heat exchanger using a hydrocarbon, isobutane (R600a)," *Int. J. Energy Res.*, vol. 32, no. 9, pp. 824–836, 2008.

[32] A. Sethi, E. Vera Becerra, and S. Yana Motta, "Low GWP R134a replacements for small refrigeration (plug-in) applications," *Int. J. Refrig.*, vol. 66, pp. 64–72, 2016.

[33] I. H. Bell, J. Wronski, S. Quoilin, and V. Lemort, "Supporting Information to Pure- and Pseudo-Pure Fluid Thermophysical Property Evaluation and the Open-Source Thermophysical Property Library CoolProp Pure and Pseudo-pure fluids Incompressible liquids , aqueous solutions and slurries," pp. 1–14.

[34] J. Remund, S. Kunz, C. Shilter, and S. Mller, "Meteonorm Version 6.0, Handbook." Part, 2010.

Chapter 3

System's Modeling and Numerical Procedure

3.1 System's Description

The proposed solar ORC system is presented in Figure 12. It consists of the following components;

- Solar thermal collector.
- PV covering the solar thermal collector absorber (In cases of FPV-T and EFPV-T collector configurations).
- Expander.
- Condenser.
- Pump.

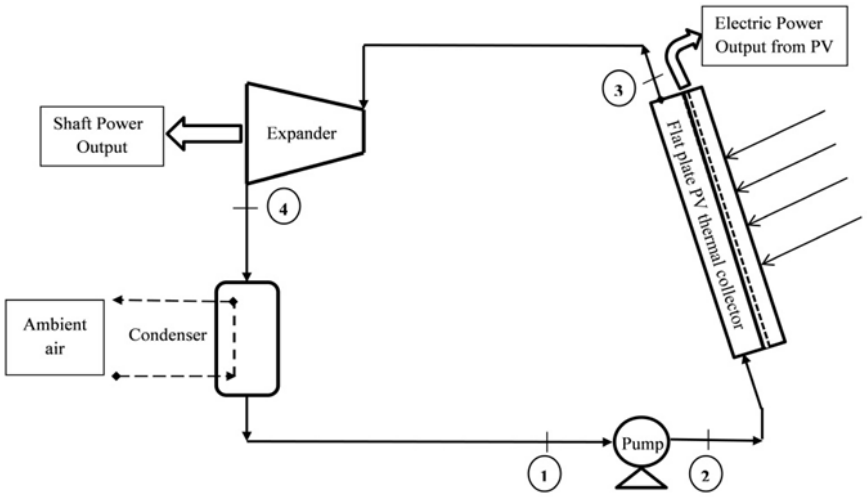

Figure 12 Schematic diagram of the proposed solar ORC system

Solar thermal collector is the key component of the system. Solar thermal collector is used as a direct vapor generator (evaporator). The cycle starts with pumping the available working fluid at condenser outlet from low pressure point or condenser pressure to higher pressure into solar thermal collector (1→2). In solar thermal collector tubes the fluid gains thermal energy, heats up and changes its phase from liquid to vapor (2→3). Fluid obtained at the outlet of the collector tube is at saturated vapor point which

then expands in the ORC expander to lower pressure, generating useful work (3→4). Now the fluid enters the condenser where it changes its phase back to saturated liquid point (4→1).

3.2 Mathematical Modeling

The detailed mathematical model of the proposed system is presented below:

- **Solar Thermal Collector**

Flat plate solar thermal collector is modeled using the thermal network procedure for a single glazed flat plate solar thermal collector (simple FPC). The model for simple FPC is modified to serve purpose for FPV-T and EFPV-T collector configurations[1]. The collector consists of top glazing, absorber, tubes, thermal insulation at the back and edges, and PV is covering the absorber plate's top surface in case of FPV-T and EFPV-T collector configurations. The schematic cross section view of the three types of solar thermal collectors, across a single tube, is presented in figure below:

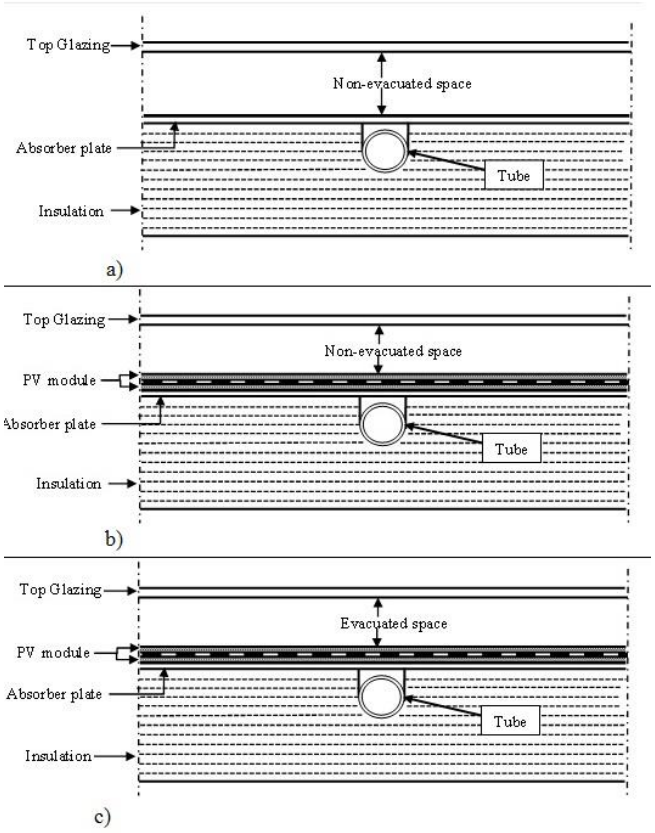

Figure 13 Schematic cross section view of the 3 types of solar thermal collectors' configurations (a) Simple FPC (b) FPV-T collector (c) EFPV-T collector

The incoming solar radiations are not completely absorbed by the solar thermal collector's absorber plate but a portion of the solar energy is lost to the environment through conduction, radiation, convection and reflection. Solar energy absorption depends on the transmittance-absorbance product $\tau\alpha$ and overall losses from the collector. The amount of solar energy absorbed by the collector absorber plate is represented in Equation (3.1).

$$Q_u = A_{abs}[I_s(\tau\alpha) - U_T(T_{abs} - T_{amb})] \quad (3.1)$$

Where:

- $\tau\alpha$ = Transmittance-absorbance product.
- I_s = Solar irradiation.
- U_T = Overall heat loss coefficient of collector (it is the sum of top heat loss coefficient U_{top}, bottom heat loss coefficient U_{back}, and edge heat loss coefficient U_{edge}. Heat loss through collector edges U_{edge} is assumed to be negligible).

In the current study, three different collector configurations are investigated so the "$\tau\alpha$" and "U_T" are estimated separately for each configuration type. The transmittance-absorbance products for FPV-T and EFPV-T configurations are evaluated as follows;

$$\tau\alpha_{FPC} = 0.81 \text{ [2]}$$

$$\tau\alpha_{FPVT} = \tau\alpha_{EFPVT} = \tau\alpha_{FPC} - (\tau_g \times \eta_{PV,r}) \text{ [3]} \quad (3.2)$$

The overall heat loss coefficients for three different collector configurations are estimated as;

$$U_{T,FPC} = U_{top,FPC} + U_{back} \quad (3.3)$$

$$U_{T,FPVT} = \left(U_{top,FPVT} + U_{back}\right) - \tau_g \times PF \times \eta_{PV,r} \times \beta_{cell} \times I_s \quad (3.4)$$

$$U_{T,EFPVT} = \left(U_{top,EFPVT} + U_{back}\right) - \tau_g \times PF \times \eta_{PV,r} \times \beta_{cell} \times I_s \quad (3.5)$$

Where:

- $U_{T,FPC}$ = Collector overall heat loss coefficient for Simple FPC.
- $U_{T,FPVT}$ = Collector overall heat loss coefficient for FPV-T.
- $U_{T,EFPVT}$ = Collector overall heat loss coefficient for EFPV-T.
- τ_g = Transmittance of top collector glazing.
- PF = Packing factor of the PV cells covering the top surface of the absorber plate.
- β_{cell} = Temperature coefficient for the solar cell efficiency.
- $\eta_{PV,r}$ = Solar cell array efficiency evaluated at reference temperature.

In case of FPV-T and EFPV-T configurations, when PV cells are covering the absorber plate, $\tau_g \times PF \times \eta_{PV} \times \beta_{cell} \times I_s$ is subtracted from the overall heat loss coefficient, as presented in Equation (3.4) and (3.5). $U_{top,FPC}$ and $U_{top,FPVT}$ respectively represent the top heat loss coefficients for simple FPC and FPV-T collector configurations while $U_{top,EFPVT}$ is for EFPV-T collector configuration. Heat loss coefficient through the collector's back U_{back} is same for all three types of configurations. Top and bottom heat loss coefficients are estimated as follows;

$$U_{top,FPC} = U_{top,FPVT} = \left[\left(\frac{1}{h_{conv,abs-g}+h_{rad,abs-g}}\right) + \left(\frac{1}{h_{conv,g-amb}+h_{rad,g-amb}}\right)\right]^{-1} \quad (3.6)$$

$$U_{top,EFPVT} = \left[\left(\frac{1}{h_{rad,abs-g}}\right) + \left(\frac{1}{h_{conv,g-amb}+h_{rad,g-amb}}\right)\right]^{-1} \quad (3.7)$$

$$U_{back} = \frac{k_{ins}}{th_{ins}} \quad (3.8)$$

Where:

- $h_{conv,abs-g}$ = Natural convective heat transfer coefficient between top glazing and absorber plate.
- $h_{rad,abs-g}$ = Radiative heat transfer coefficient between absorber plate and top glazing.

- $h_{conv,g-amb}$ = Convection heat transfer coefficient from top glazing to the ambient [4].
- $h_{rad,g-amb}$ = Radiation heat transfer coefficient from top glazing to the ambient.
- k_{ins} = Insulation thermal conductivity.
- th_{ins} = Insulation thickness.

As in the case of EFPV-T configuration, air between absorber plate and glazing is sucked out hence the natural convective heat transfer term $h_{conv,abs-g}$ from absorber to top glazing is ignored in calculating the collector's top heat loss coefficient. The four heat transfer coefficients mentioned above are calculated as follows;

$$h_{conv,abs-g} = \frac{(Nu_{air} \times k_{air})}{L_{asb-g}} \tag{3.9}$$

$$h_{rad,abs-g} = \frac{[\sigma_{stf}(T_{abs}^2 + T_g^2) \times (T_{abs} + T_g)]}{\left[1/\varepsilon_{abs} + 1/\varepsilon_g - 1\right]} \tag{3.10}$$

$$h_{rad,g-amb} = \varepsilon_g \times \sigma_{stf}\left(T_g^2 + T_{sky}^2\right) \times \left(T_g + T_{sky}\right) \tag{3.11}$$

$$h_{conv,g-amb} = 5.7 + (3.8 \times w) \tag{3.12}$$

Where:

- Nu_{air} = Nusselt number of the air present between absorber and glazing.
- k_{air} = Thermal conductivity of the air present between absorber plate and top glazing.
- L_{asb-g} = Distance between absorber plate and glazing.
- ε_{abs} = Emissivity of absorber plate.
- ε_g = Emissivity of top glazing.
- σ_{stf} = Stefan-Boltzmann constant.
- w = Wind speed.

Working fluid flowing in the collector tubes beneath the absorber gains heat that is being transferred from hot absorber plate. It is called the useful heat gain and is calculated as[5];

$$Q_u = A_{abs}F_r\left[I_s(\tau\alpha) - U_T\left(T_{wf,in} - T_{amb}\right)\right] \tag{3.13}$$

Where:

- F_r = Heat removal factor.
- $T_{wf,in}$ = Working fluid's inlet temperature.

Heat removal factor is calculated as [5], [6];

$$F_r = \frac{\dot{m}_{wf}C_p}{A_{abs}U_T}\left[1 - \exp\left(\frac{-A_{abs}U_T F`}{\dot{m}_{wf}C_p}\right)\right] \tag{3.14}$$

Where:

- $\dot{m}_{wf}$ = Fluid mass flow rate in collector tubes.
- $F`$ = Collector efficiency factor
- C_p = Heat capacity of the fluid

$$F` = \frac{(U_T)^{-1}}{W[U_T(D_{out}+(W-D_{out})F)]^{-1}+(C_b)^{-1}+\left(\pi D_{in}h_{wf}\right)^{-1}} \tag{3.15}$$

Where:

- D_{out} = Collector tube outer diameter.
- D_{in} = Collector tube inner diameter.
- W = Spacing between tubes.
- C_b = PV-absorber bond conductance which is neglected $((C_b)^{-1} = 0)$
- F = Fin efficiency and can be determined as;

$$F = \frac{\tanh\left[m\left(W - {D_{out}}/{2}\right)\right]}{m\left(W - {D_{out}}/{2}\right)} \tag{3.16}$$

where the coefficient m for simple FPC is determined by Equation (3.17) while for FPV-T and EFPV-T configurations both absorber and PV cell thermal conductivities are considered in calculating coefficient m, Equation (3.18) [3], [7], [8].

$$m = m_{FPC} = \sqrt{\frac{U_T}{k_{abs} th_{abs}}} \tag{3.17}$$

$$m = m_{FPVT} = m_{EFPVT} = \sqrt{\frac{U_T}{k_{abs} th_{abs} \times k_{PV} th_{PV}}} \tag{3.18}$$

In Equation (3.15) for collector fin efficiency, h_{wf} is the convective heat transfer coefficient of working fluid flowing in the collector tubes. The method to determine convective heat transfer coefficient is different for single phase flow and multiphase flow, as the working fluid changes its phase in collector tubes.

Single phase flow

Several heat transfer books [9], [10] has presented the heat transfer coefficient evaluation method for fluids in single phase flow and the same method is being followed in this study. Single phase heat transfer coefficient is determined as;

$$h_{wf,sp} = \frac{Nu \times k_{wf}}{D_{in}} \tag{3.19}$$

For fully developed laminar flow, in circular tube;

$$Nu = 4.36, \quad Re < 2300 \tag{3.20}$$

For fully developed turbulent flow, in circular tube;

$$Nu = \frac{\frac{f}{8}(Re - 1000)Pr}{1 + 12.7\left(\frac{f}{8}\right)^{0.5}\left(Pr^{2/3} - 1\right)}, \quad (3 \times 10^3 < Re < 5 \times 10^6), (0.5 < Pr < 2000) \tag{3.21}$$

Where:

- Re = Reynolds number.
- Pr = Prandtl number.
- f = Single phase liquid friction factor.

Reynolds number is calculated as;

$$Re = \frac{G \times D_{in}}{\mu} \tag{3.22}$$

Where:

- $\mu =$ Fluid dynamic viscosity.
- $G =$ Mass flux.

Single phase liquid friction factor and is estimated as [11];

$$f = (0.79 \ln Re - 1.64)^{-2}, \qquad 10^4 < Re < 10^6 \tag{3.23}$$

Multi-phase flow

Correlation presented in [12], for horizontal and vertical flows in tubes is implemented here to evaluate the heat transfer coefficient in multiphase flow $h_{wf,mp}$. These correlations are the mathematical version of its earlier graphical chart correlations in [13].

Initially, Froude number is evaluated which will help determine if the surface of the tube is partly dry or fully wet.

$$Fr = \frac{G^2}{\rho_l^2 \times g \times D_{in}} \tag{3.24}$$

If the orientation of the tube is vertical then it does not depend on the Froude number and its surface is considered to be fully wet. If the tube's orientation is horizontal then following 2 cases are possible

- $Fr < 0.04$ - Surface of tube is partly dry
- $Fr > 0.04$ - Surface of tube is fully wet

Dimensionless parameter N is calculated based on the following conditions;

- For vertically oriented tubes (under all Fr values) and horizontally orientated tubes if $Fr > 0.04$;

$$N = Co \tag{3.25}$$

- For horizontal tubes when $Fr < 0.04$;

$$N = 0.38Fr^{-0.3}Co \tag{3.26}$$

where Co is dimensionless parameter called convection number and is evaluated as follows;

$$Co = \left(\frac{1}{x} - 1\right)^{0.8} \left(\frac{\rho_{vap}}{\rho_l}\right)^{0.5} \tag{3.27}$$

Following 3 cases are defined to calculate nucleate boiling factor ψ_{nb};

- *Case 1:* $N > 1$

$$\psi_{nb} = 230\, Bo^{0.5} \quad \rightarrow \quad Bo > 0.3 \times 10^{-4} \tag{3.28}$$

$$\psi_{nb} = 1 + 46\, Bo^{0.5} \quad \rightarrow \quad Bo < 0.3 \times 10^{-4} \tag{3.29}$$

where Bo is the boiling number and is evaluated as;

$$Bo = \frac{\phi}{Gh_{fg}} \tag{3.30}$$

where ϕ and h_{fg} represents the heat flux and heat of vaporization, respectively.

- *Case 2:* $0.1 < N < 1$

$$\psi_{nb} = F\, Bo^{0.5} exp(2.74N^{-0.1}) \tag{3.31}$$

- *Case 3:* $N < 0.1$

$$\psi_{nb} = F\, Bo^{0.5} exp(2.47N^{-0.15}) \tag{3.32}$$

Where:

$$F = 14.7, \quad \text{if } Bo > 0.0011 \tag{3.33}$$

$$F = 15.43, \quad \text{if } Bo < 0.0011 \tag{3.34}$$

Convective boiling factor is determined as follows;

$$\psi_{cb} = 1.8\, N^{-0.8} \tag{3.35}$$

To determine the multiphase heat transfer coefficient $h_{wf,mp}$, the larger value of ψ_{cb} or ψ_{nb} is multiplied with the heat transfer coefficient of liquid phase $h_{wf,l}$.

$$h_{wf,mp} = \psi \times h_{wf,l} \tag{3.36}$$

Where Dittus-Boelter equation[12] is used to evaluate the heat transfer coefficient of liquid phase $h_{wf,l}$.

- **Expander**

The output expansion work is evaluated by using the following formula;

$$\dot{W}_{exp-i} = \dot{m}_{wf} \times \left(h_3 - h_{4,i}\right) \tag{3.37}$$

$$\dot{W}_{shaft} = \left(\dot{m}_{wf} \times (h_3 - h_4)\right) \times \eta_{exp-mech} \tag{3.38}$$

Where:

- $\dot{W}_{exp-i}$ = Expander's isentropic expansion work.
- $\dot{W}_{shaft}$ = Shaft power.
- h_3 = Enthalpy at expander inlet.
- h_4 = Actual enthalpy at expander outlet.
- $h_{4,i}$ = Isentropic enthalpy at expander outlet.
- $\eta_{exp-mech}$ = Expander's mechanical efficiency.

- **Condenser**

Fluid entering the condenser can either be superheated, saturated vapor or mixture. So the total heat rejected in condenser consists of latent heat rejection and sensible heat rejection part. Condensation heat is evaluated using the following formula;

$$\dot{Q}_{cond} = \dot{m}_{wf} \times \left(h_3 - h_{vap,cond}\right) + \dot{m}_{wf} \times \left(h_{vap,cond} - h_1\right) \tag{3.39}$$

Where:

- $h_{vap,cond}$ = Enthalpy at saturated vapor point at condenser temperature.
- h_1 = Enthalpy at condenser outlet or saturated liquid point at condenser temperature.

- **Pump**

As pump is used to compress the fluid, which consumes power and is called work input of the cycle. This input work is determined as[14];

$$\dot{W}_{pump} = \dot{m}_{wf} \times \left(\frac{\nu_{pump-in}(P_{evap} - P_{cond})}{\eta_{pump-i}} \right) \quad (3.40)$$

Where:

- P_{evap} = Evaporator pressure
- P_{cond} = Condenser pressure
- $\nu_{pump-in}$ =Fluid's specific volume at pump inlet

  η_{pump-i} = Pump isentropic efficiency

3.3 Numerical Procedure

Mathematical model developed in the previous section is coded using MATLAB simulation software. In this section, the complete simulation procedure and iteration process of the MATLAB code is explained. The block diagram presented in Figure 14 displays the basic structure of the developed MATLAB code and complete numerical procedure is presented in Figure 15.

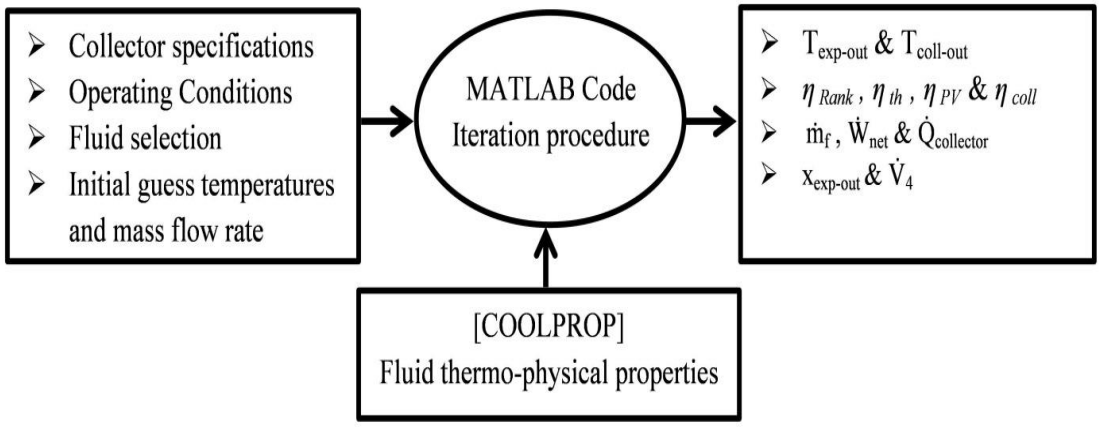

Figure 14 Block diagram for MATLAB simulation model

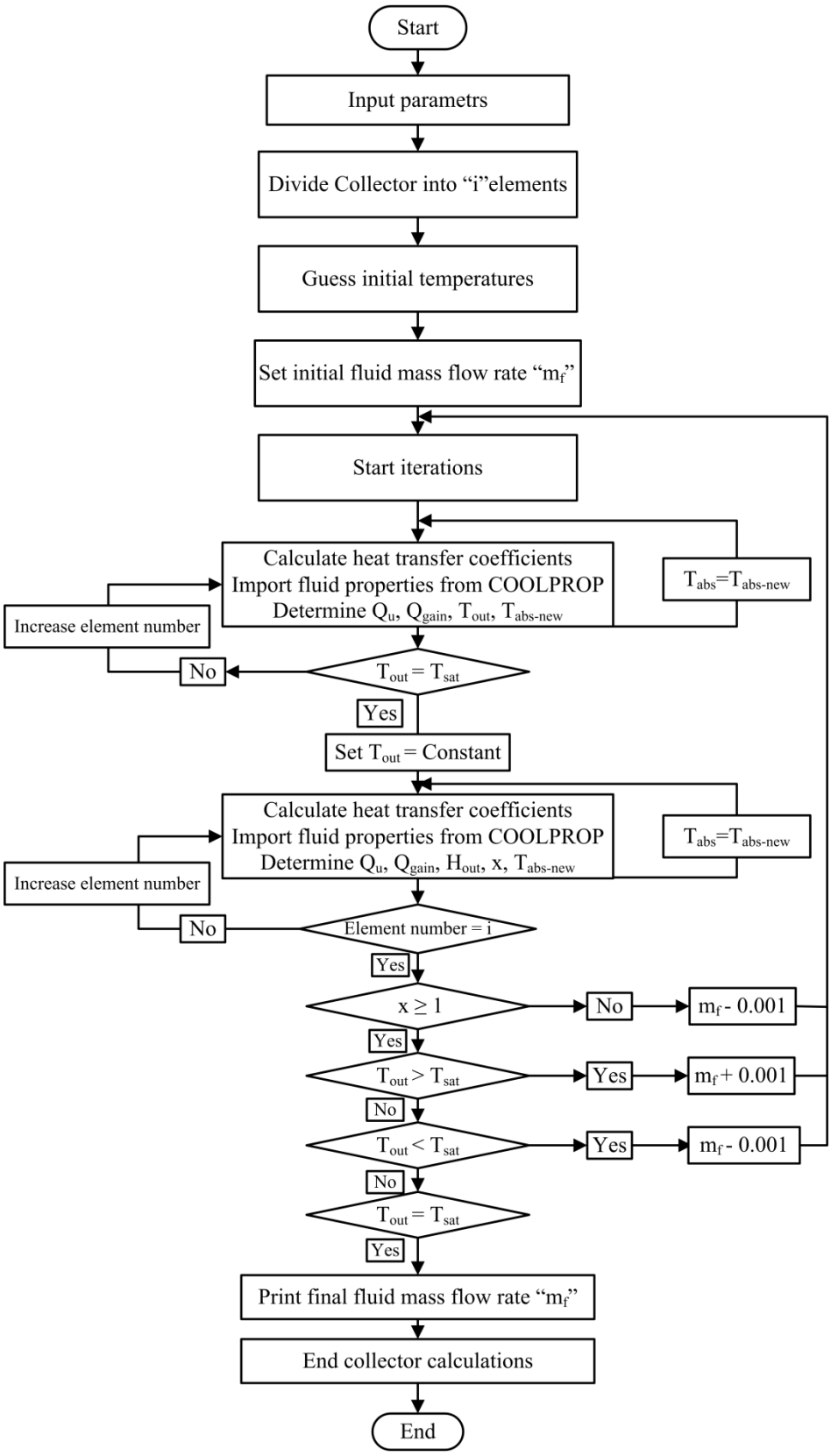

Figure 15 Simulation model flow chart

In the simulation, input parameters such as collector and PV module specifications, system operating conditions, expander isentropic and mechanical efficiencies, pump isentropic efficiency and ambient conditions remain constant. Working fluids thermo-physical properties are imported using COOLPROP software[15]. Solar collector and PV module's specifications[8] are presented in Table 2.

Initially the iteration process starts with the constant input parameters, and fluid properties at the initial input conditions are imported from COOLPROP. With all the input data available, the simulation starts with calculating pump work using Equation (3.40). Enthalpy at pump inlet is determined at condenser pressure and saturated liquid point (vapor quality = 0). As pump work and inlet enthalpy are already determined, pump outlet enthalpy is calculated using Equation (3.41). The collector inlet temperature is determined at pump outlet enthalpy and given evaporation pressure.

$$h_{pump-out} = h_2 = h_{pump-in} + \left(\frac{\dot{W}_{pump}}{\dot{m}_{wf}}\right) \tag{3.41}$$

Table 2 Solar collector and PV module specifications

Specification	Value
Collector area (A)	6.96 m^2
Absorber plate emissivity	0.20
Top glazing emissivity	0.90
No. of glazing (N)	1
Simple FPC effective transmission-absorption product ($\tau\alpha_{col}$)	0.81
Collector's tilt	0° (Horizontal)
PV module reference efficiency (η_{ref})	12 %
Packing factor (PF)	85 %
FPV-T and EFPVT effective transmission-absorption product ($\tau\alpha_{PV}$)	0.699
PV cell temperature coefficient (β_{PVref})	$-0.0045\ °C^{-1}$

At this calculated inlet temperature, the pressurized working fluid enters the solar collector tubes. The simulation considers the serpentine tube of the collector to be a single long tube, and for further analysis it is divided into small elements. For each element the temperatures of absorber, top glazing, tube and back insulation are uniform, while the working fluid's temperature flowing in the collector tube increases along its

length. Simulation starts with the first element and calculates heat transfer and heat loss coefficients. For simple FPC and FPV-T collector configurations, the overall heat loss coefficient of the collector is calculated using Equation (3.3) and Equation (3.4), respectively. In case of EFPV-T collector configuration, overall heat loss coefficient is determined using Equation (3.5), where natural convective heat transfer coefficient between PV-absorber plate and top glazing is zero. Heat transfer coefficients are calculated utilizing Equation (3.9) to Equation (3.12).

To determine the single phase heat transfer coefficient of the fluid, Reynolds number is initially calculated that will define the fluid flow type as laminar or turbulent. Nusselt number is calculated depending on the fluid flow type, and consequently single phase heat transfer coefficient is evaluated using Equation (3.19). Useful heat gain Q_u of the working fluid is determined from Equation (3.13) and new absorber temperature is calculated utilizing the useful heat gain.

The useful heat gain evaluated by using Equation (3.13) denotes the heat gain for the entire tube length of the collector. Now, useful heat rate (Equation (3.42)) is assessed by dividing the useful heat gain by $\pi D_{in} L_t$, where πD_{in} indicates the collector tube's surface perimeter and L_t is the total tube length. The useful heat rate is utilized to evaluate heat gain for each element by using Equation (3.43).

$$Q_{rate} = {Q_u}/{\pi D_{in} L_t} \tag{3.42}$$

$$Q_{gain} = Q_{rate} \times \pi D_{in} \int_0^{L_t} dx \tag{3.43}$$

Heat gain is calculated for the first element which is then used to determine the fluid's temperature at the outlet of that same element as;

$$T_{wf,out} = T_{wf,in} + \frac{Q_{gain}}{\dot{m}_{wf} C_p} \tag{3.44}$$

The simulation evaluates the difference between the newly calculated outlet temperature and its previous value and new absorber temperature and its previous value. This difference is then compared with the convergence criteria, which is set at 0.01˚C. If the difference is less than the set criteria, the iteration stops and new temperature values are

saved and enter the second loop; otherwise the whole procedure is repeated in the first loop using the newly calculated temperatures. In the second loop, the new fluid's outlet temperature of the first element is checked if it has reached the fluid's saturation temperature at the corresponding evaporation pressure. If the saturation point has not reached, the program will keep adding another element and the same process is repeated until the saturation temperature point is obtained at the outlet, and two phase flow starts in the collector tube.

In two phase flow the whole iteration process remains the same, except for calculating the single phase flow heat transfer coefficient flow boiling calculations are taken into account. The fluid outlet temperature is constant and fluid's enthalpy at the outlet of each element and corresponding vapor quality are calculated as;

$$h_{out} = h_{in} + {Q_{gain}}/{\dot{m}_{wf}} \tag{3.45}$$

$$x = \frac{h_{out} - h_l}{h_{vap} - h_l} \tag{3.46}$$

The process continue to increase the tube length and add new element till the vapor quality reaches 1 (saturated vapor point). If at the final element (end of collector tube), vapor quality is still less than 1 then the initially assumed mass flow rate is decreased by 0.0001 kg/s and the whole program starts over again with this new mass flow rate. The iteration procedure continues to decrease the mass flow rate till saturated vapor ($x = 1$) is obtained at the outlet of the collector tube. If vapor quality reaches 1 before the final element and the fluid enters superheated phase then the mass flow rate is increased by 0.0001 kg/s and the whole program starts over again till saturated vapor is obtained at collector outlet.

The expander receives the working fluid at saturated vapor point where it expands down to the cycle's lower pressure (condensation pressure). The expander's isentropic and mechanical efficiencies are constant and the output shaft power is calculated as;

$$\dot{W}_{shaft} = \left(\dot{m}_{wf} \times (h_3 - h_4)\right) \times \eta_{exp-mech} \tag{3.47}$$

where;

$$h_4 = h_3 - \left(\eta_{exp-i} \times \left(h_3 - h_{4,i}\right)\right) \tag{3.48}$$

At expander's outlet temperature and vapor fraction of working fluid is determined at the expander outlet enthalpy h_4 and corresponding condenser pressure P_{cond}. Cycle's net work output is calculated as;

$$\dot{W}_{net} = \dot{W}_{exp} - \dot{W}_{pump} \tag{3.49}$$

Now volume flow rate is evaluated at the outlet of the expander using the fluid's density and mass flow rate.

$$\dot{V}_{exp-out} = \left(\frac{\dot{m}_{wf}}{\rho_{exp-out}}\right) \times 3600 \tag{3.50}$$

In the end, the code evaluates solar collector collection efficiency, Rankine cycle efficiency, system thermal efficiency and PV electrical efficiency.

$$\eta_{col} = \frac{Q_{abs}}{I_s A_{col}} \tag{3.51}$$

$$\eta_{Rank} = \frac{\dot{W}_{exp-i}}{Q_{abs}} \tag{3.52}$$

$$\eta_{th} = \frac{\dot{W}_{exp} - \dot{W}_{pump}}{I_s A_{col}} \tag{3.53}$$

$$\eta_{PV} = \eta_{PV,r}\,[1 - \beta_{cell}\,(T_{PV} - T_r)] \tag{3.54}$$

To investigate the overall performance of the system, system overall electrical output and overall electrical efficiency have been introduced and are calculated as[16];

$$\eta_{sys,ele} = \frac{\dot{W}_{sys,ele} - \dot{W}_{cool}}{I_s A_{col}} \tag{3.55}$$

$$\dot{W}_{sys,ele} = \dot{W}_{net} \Big/ A_{col} + \dot{W}_{PV} \tag{3.56}$$

where $\eta_{sys,ele}$ is the system overall electrical efficiency (%) and $\dot{W}_{sys,ele}$ is system overall electrical output (W/m^2). $\dot{W}_{cool}$ shows the air pump power consumption (W/m^2) that circulates the air in condenser and its value is taken as 2% of the incident solar

insolation[17]. $\dot{W}_{PV}$ represents the electrical output of PV (W/m^2) and is calculated as follows;

$$\dot{W}_{PV} = I_s \times \tau_g \times \eta_{PV} \times PF \tag{3.57}$$

3.4 Model Validation

The collector's mathematical model presented in section 3.2.1 is validated against the theoretical and experimentally validated results of [18]. Simulation results are

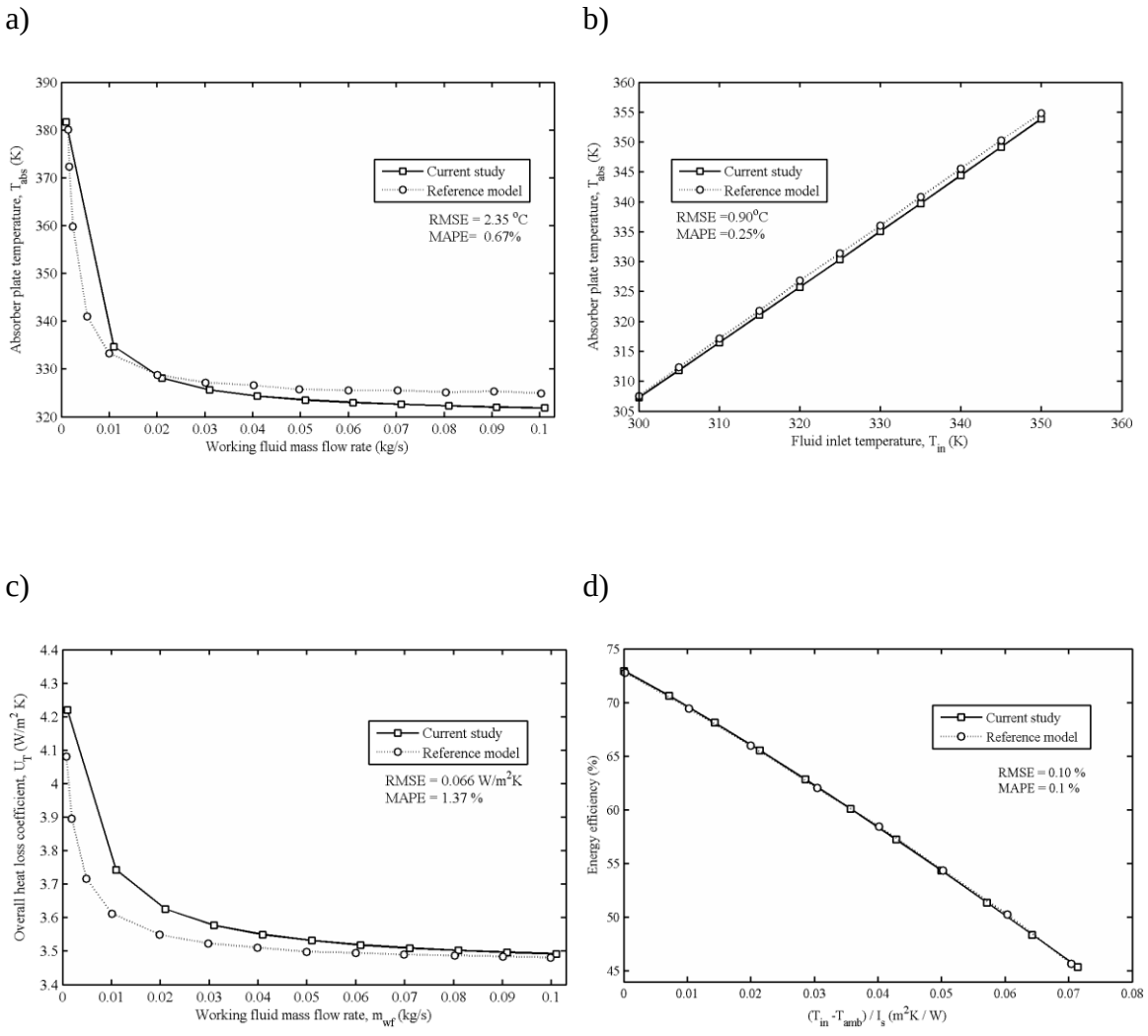

Figure 16 Model validation a) Absorber temperature versus mass flow rate b) Absorber temperature versus fluid inlet temperature c) Collector overall heat loss coefficient versus mass flow rate d) Collector energy efficiency versus $(T_{in} - T_{amb})/I_s$

obtained by utilizing the operating conditions and input parameters as those in [18] . For the statistical analysis, following two parameters are used [19], [20].

- RMSE (root mean squared error)

$$RMSE = \sqrt{\sum_{i=1}^{n} \frac{(y_{simulated,i} - y_{reference,i})^2}{n}} \quad (3.58)$$

- MAPE (mean absolute percent error)

$$MAPE = \frac{100\%}{n} \sum \left| \frac{y_{simulated} - y_{reference}}{y_{reference}} \right| \quad (3.59)$$

It can be observed from Figure 16(c) that collector overall heat loss coefficient versus mass flow rate shows the maximum mean absolute percent error of 1.37 %. The simulation results in current study shows a good agreement with the results in [18].

3.5 Working Fluids Selection

The initial criterion for the working fluids' selection is based on;

- Zero ozone depletion potential (ODP).
- Minimum allowable P_{cond} of 0.005 MPa at 298 K temperature[21].
- Dry fluids to avoid formation of moisture content in steam during expansion.

Five potential HCs, HFC and HFO working fluids i.e. R600, R600a, R601, R245fa, and R1234ze(E) that are most commonly found in literature have been selected based on above criteria, and are shown in Table 3 and Table 4.

Table 3 Working fluid physical, safety and environmental data

Refrigerants		Physical data				Safety data	Environmental data			Source
		Molecular mass (kg/kmol)	T_{bp} [K]	T_{crit} [K]	P_{crit} [MPa]	ASHRAE safety group	Atmospheric lifetime (yr)	ODP	GWP (100yr)	
1	R600	58.122	272.65	425	3.796	A3	0.018	0	~20	[14], [22], [23]
2	R600a	58.122	261.45	408	3.647	A3	0.019	0	~20	[14], [22]–[24]
3	R601	72.149	309.21	469.75	3.37	A3	0.01	0	11	[14], [23]–[25]
4	R245fa	134.05	288.25	427.15	3.65	B1	7.6	0	1030	[22], [23], [25]–[28]
5	R1234ze(E)	114.04	254.13	382.46	3.634	A2L	0.05	0	6	[24], [25]

Table 4 Practical limitation for condenser pressure

Refrigerants		Condensing Pressure at 298 K	
		P_{cond} (MPa)	T_{cond} (K)
1	R600	0.243	298
2	R600a	0.351	298
3	R601	0.068	298
4	R245fa	0.148	298
5	R1234ze(E)	0.499	298

3.6 Operating Conditions

Operating conditions and turbine and pump efficiencies for the saturated solar ORC are presented in Table 5. A subcritical type ORC has been considered in which fluid goes through a phase change before it is superheated. Weather data for Islamabad, Pakistan obtained from Meteonorm software revealed that during the month of June average ambient air temperature and solar insolation recorded is the highest. Simulations are performed on the weather data of June, when monthly average ambient temperature of 304 K is recorded and solar irradiation for the most part of the daily sunshine-hours

Table 5 Superheated solar ORC operating conditions

ORC type	Subcritical
Solar irradiation	750 W/m^2
Ambient temperature	304 K
Wind speed	1.12 m/sec
Condensation temperature	310 K
Maximum evaporation pressure	1.5 MPa
Maximum pressure ratio	3.5
Expander isentropic efficiency	70 %
Expander mechanical efficiency	95 %
Pump isentropic efficiency	80 %

remain around 750 W/m^2. As ambient air is used to condense the incoming working fluid into saturated liquid in the condenser, the fluid's condensing temperature is set 6℃

above ambient at 310 K. This condensing temperature and the corresponding pressure for the working fluids remain constant throughout the simulations. Evaporating pressure in solar thermal collector can not exceed 1.5 MPa. Maximum pressure ratio of the cycle is taken as 3.5, as common pressure ratio values for most of the ORC systems range from 3-4 [14], [29].

Summary

Detailed description and mathematical model of the saturated solar ORC system is presented in this chapter. The system comprises of pump, condenser, expander and evacuated flat plate photovoltaic-thermal (EFPV-T) collector. The EFPV-T collector is used as a direct vapor generator in solar ORC. A detailed mathematical model for the solar thermal collector has been established and presented in this chapter. Thermal network model has been followed for collector modeling, while equations for single phase flow and multi-phase flow have also been incorporated. MATLAB computer software is used to code the model while thermo-physical data of fluids have been imported from COOLPROP software. After the mathematical model, the numerical procedure that will be followed in MATLAB computations has been explained. The collector model is validated against theoretical and experimentally validated results, and it showed good agreement with the reference model. Five working fluids are initially selected based on their low adverse environmental impacts and allowable condensing pressure. In the end, operating conditions and efficiencies of different system components are presented.

References

[1] L. W. Ft, “EXTENSION OF THE HOTTEL-WHILLIER MODEL TO THE ANALYSIS OF COMBINED PHOTOVOLTAIC / THERMAL FLAT PLATE COLLECTORS,” vol. 22, pp. 361–366, 1979.

[2] H. U. Helvaci and Z. A. Khan, “Mathematical modelling and simulation of multiphase flow in a flat plate solar energy collector,” *Energy Convers. Manag.*, vol. 106, pp. 139–150, 2015.

[3] H. A. Zondag, D. W. D. E. Vries, W. G. J. V. A. N. Helden, R. J. C. V. A. N. Zolingen, and A. A. V. A. N. Steenhoven, “THE THERMAL AND ELECTRICAL YIELD OF A PV-THERMAL COLLECTOR,” vol. 72, no. 2, pp. 113–128, 2002.

[4] W. H. McAdams, *Heat Transmission: William H-McAdams*. McGraw-hill, 1954.

[5] John A Duffie and W. A. Beckman, *Solar Engineering of Thermal Processes Solar Engineering*. 2013.

[6] H. Hottel and A. Whillier, “Evaluation of flat-plate solar collector performance,” in *Trans. Conf. Use of Solar Energy;()*, 1955, vol. 3.

[7] F. Ghani, M. Duke, and J. K. Carson, “Effect of flow distribution on the photovoltaic performance of a building integrated photovoltaic / thermal (BIPV / T) collector,” *Sol. Energy*, vol. 86, no. 5, pp. 1518–1530, 2012.

[8] A. Fudholi, K. Sopian, M. H. Yazdi, M. Hafidz, A. Ibrahim, and H. A. Kazem, “Performance analysis of photovoltaic thermal (PVT) water collectors,” *ENERGY Convers. Manag.*, vol. 78, pp. 641–651, 2014.

[9] Y. A. Cengel, S. Klein, and W. Beckman, *Heat transfer: a practical approach*, vol. 141. McGraw-Hill New York, 1998.

[10] T. L. Bergman, F. P. Incropera, D. P. DeWitt, and A. S. Lavine, *Fundamentals of heat and mass transfer*. John Wiley & Sons, 2011.

[11] B. S. Petukhov, “Heat transfer and friction in turbulent pipe flow with variable physical properties,” in *Advances in heat transfer*, vol. 6, Elsevier, 1970, pp. 503–564.

[12] M. M. Shah, “A new correlation for heat transfer during boiling flow through pipes,” no. November, 2017.

[13] C. Paper and M. M. Shah, “Chart correlation for saturated boiling heat transfer : Equations and further study,” no. January 1982, 2015.

[14] B. F. Tchanche, G. Papadakis, G. Lambrinos, and A. Frangoudakis, “Fluid selection for a low-temperature solar organic Rankine cycle,” *Appl. Therm. Eng.*, vol. 29, no. 11–12, pp. 2468–2476, 2009.

[15] I. H. Bell, J. Wronski, S. Quoilin, and V. Lemort, “Supporting Information to Pure- and Pseudo-Pure Fluid Thermophysical Property Evaluation and the Open-Source Thermophysical Property Library CoolProp Pure and Pseudo-pure fluids Incompressible liquids , aqueous solutions and slurries,” pp. 1–14.

[16] G. Kosmadakis, D. Manolakos, and G. Papadakis, “Simulation and economic analysis of a CPV/thermal system coupled with an organic Rankine cycle for increased power generation,” *Sol. Energy*, vol. 85, no. 2, pp. 308–324, 2011.

[17] G. Mittelman, A. Kribus, and A. Dayan, “Solar cooling with concentrating photovoltaic/thermal (CPVT) systems,” *Energy Convers. Manag.*, vol. 48, no. 9, pp. 2481–2490, 2007.

[18] F. Jafarkazemi and E. Ahmadifard, “Energetic and exergetic evaluation of fl at plate solar collectors,” *Renew. Energy*, vol. 56, pp. 55–63, 2013.

[19] G. Notton, C. Cristofari, M. Mattei, and P. Poggi, “Modelling of a double-glass photovoltaic module using finite differences,” *Appl. Therm. Eng.*, vol. 25, no. 17–18, pp. 2854–2877, 2005.

[20] L. M. Ayompe, A. Duffy, S. J. McCormack, and M. Conlon, “Validated TRNSYS model for forced circulation solar water heating systems with flat plate and heat

pipe evacuated tube collectors," *Appl. Therm. Eng.*, vol. 31, no. 8–9, pp. 1536–1542, 2011.

[21] J. Bao and L. Zhao, "A review of working fl uid and expander selections for organic Rankine cycle," *Renew. Sustain. Energy Rev.*, vol. 24, pp. 325–342, 2013.

[22] Z. Q. Wang, N. J. Zhou, J. Guo, and X. Y. Wang, "Fluid selection and parametric optimization of organic Rankine cycle using low temperature waste heat," *Energy*, vol. 40, no. 1, pp. 107–115, 2012.

[23] B. Saleh, G. Koglbauer, M. Wendland, and J. F. Ã, "Working fluids for low-temperature organic Rankine cycles," vol. 32, pp. 1210–1221, 2007.

[24] U. Helvaci and Z. Khan, "Thermodynamic modelling and analysis of a solar organic Rankine cycle employing thermofluids," *Energy Convers. Manag.*, vol. 138, Feb. 2017.

[25] H. Zhai, L. Shi, and Q. An, "In fl uence of working fl uid properties on system performance and screen evaluation indicators for geothermal ORC (organic Rankine cycle) system," *Energy*, 2014.

[26] L. Li, Y. T. Ge, X. Luo, and S. A. Tassou, "Thermodynamic analysis and comparison between CO 2 transcritical power cycles and R245fa organic Rankine cycles for low grade heat to power energy conversion," vol. 106, pp. 1290–1299, 2016.

[27] X. D. Wang, L. Zhao, J. L. Wang, W. Z. Zhang, X. Z. Zhao, and W. Wu, "Performance evaluation of a low-temperature solar Rankine cycle system utilizing R245fa," *Sol. Energy*, vol. 84, no. 3, pp. 353–364, 2010.

[28] P. Gang, L. Jing, and J. Jie, "Working Fluid Selection for Low Temperature Solar Thermal Power Generation with Two-stage Collectors and Heat Storage Units."

[29] G. Kosmadakis *et al.*, "Experimental testing of a low-temperature organic Rankine cycle (ORC) engine coupled with concentrating PV / thermal collectors : Laboratory and field tests To cite this version : HAL Id : hal-01457277

(ORC) engine coupled with concentrating PV / ther," *Energy*, vol. 117, pp. 222–236, 2017.

Chapter 4

Results and Discussion

4.1 Simulation Results and Discussion

For the thermodynamic and performance analysis of the proposed low temperature saturated solar ORC system simulations are executed at increasing pressure ratios (1.5 – 3.5) and three different collector configurations as described in chapter 2. Pressure ratio is dictated by varying evaporating pressure, as condensing temperature and the corresponding pressure is kept constant throughout the simulations.

Operating pressure (evaporating pressure) of 1.5 MPa (15bar) is the maximum allowable limit for conventional domestic flat plate solar thermal collectors, as previously stated. It means that solar ORC working fluids that utilizes domestic solar thermal collector as an evaporator (direct vapor generator) can not exceed the maximum cycle pressure of 1.5MPa. Evaporating pressures of the working fluids are investigated at different pressure ratio points (1.5-3.5), as shown in Figure 17. The dashed horizontal line in Figure 17 is the maximum allowable evaporating pressure limit (1.5MPa) in the solar thermal collector. So the evaporating pressure points for the working fluids that fall below 1.5MPa limit are acceptable. Figure 17 revealed that for working fluids R600a and R1234ze(E) PR points upto 3 and 2 could be achieved, respectively. R600, R601 and R245fa present acceptable evaporating pressures at all PR points (1.5-3.5).

In the following sections, different performance parameters have been discussed in detail. In case of R600a, and R1234ze(E) only the allowable evaporating pressures that are below the 1.5MPa limit will be considered for analysis.

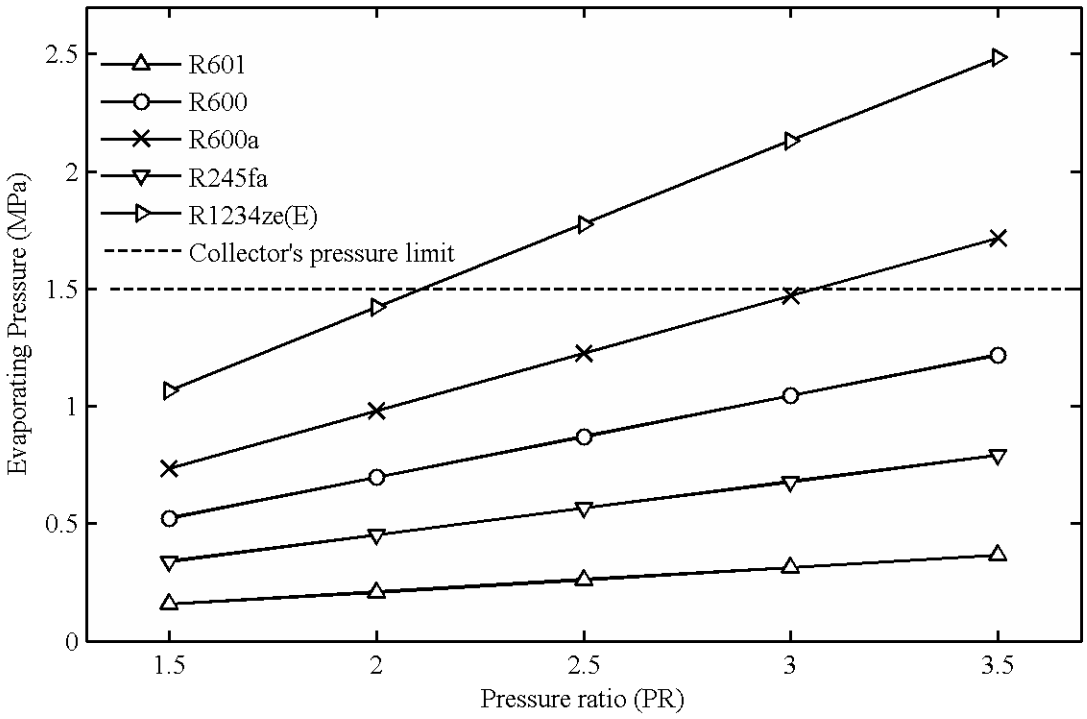

Figure 17 Working fluids evaporating pressures at corresponding pressure ratios

4.1.1 Solar thermal collector Performance Analysis:

Performance parameters of the solar collector are investigated in this section. Collection efficiency, heat absorbed in collector, and overall heat loss coefficient are presented in Figures 19-21. Figure 19 presents the collector's collection efficiency versus pressure ratio under three collector configurations for five working fluids. Collection efficiency of the collector is observed to be decreasing with increasing pressure ratio; the reason is that at higher pressure ratio the fluid's evaporation temperature increases hence the absorber plate temperature rises, consequently resulting in higher thermal losses to the ambient and less heat is absorbed in the collector, as presented in Figure 20.

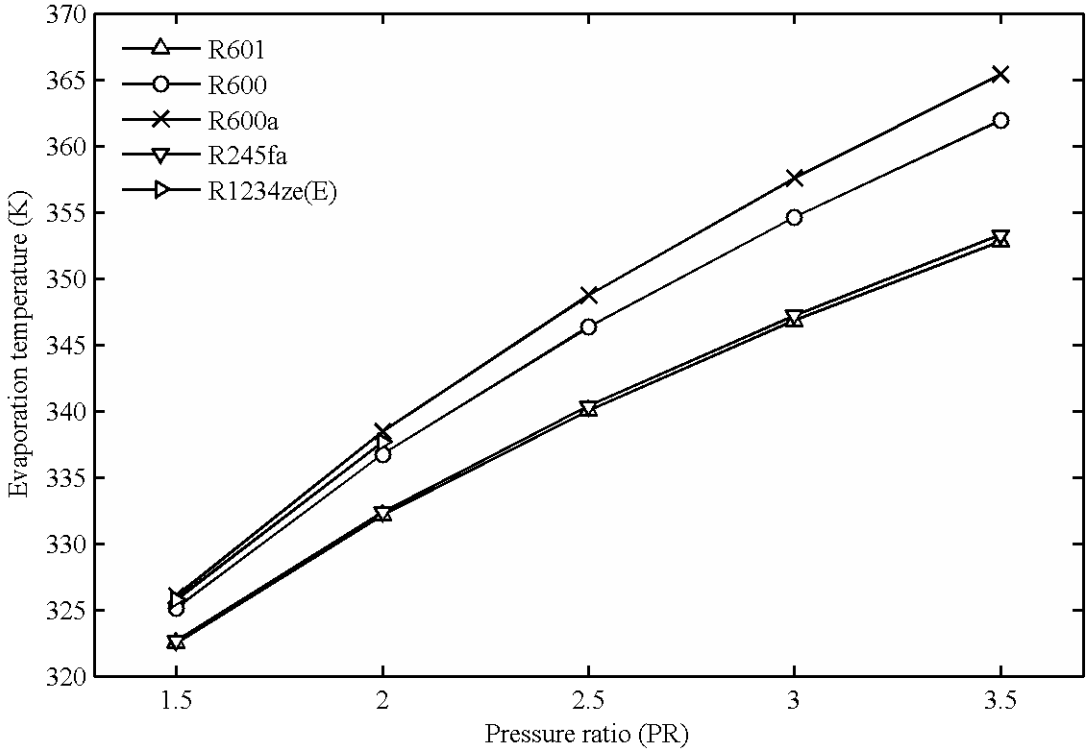

Figure 18 Working fluids evaporation temperatures at different PR

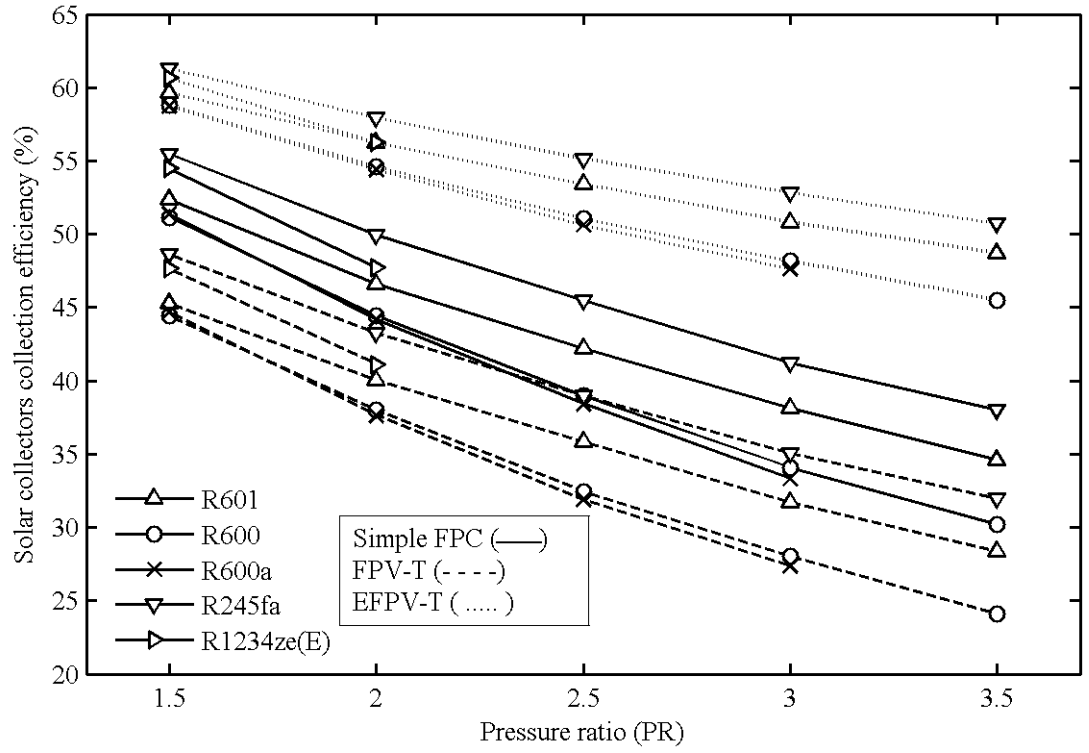

Figure 19 Solar collector collection efficiency at various pressure ratios and three different collector configurations

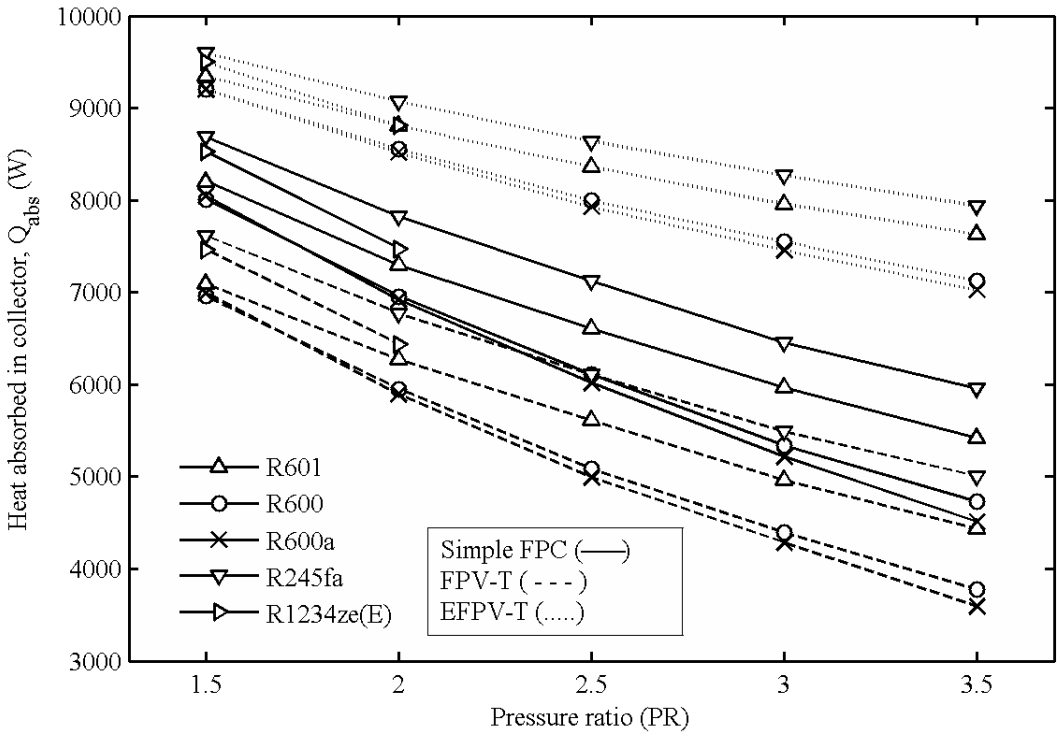

Figure 20 Heat absorbed in collector under various pressure ratios and three different collector configurations

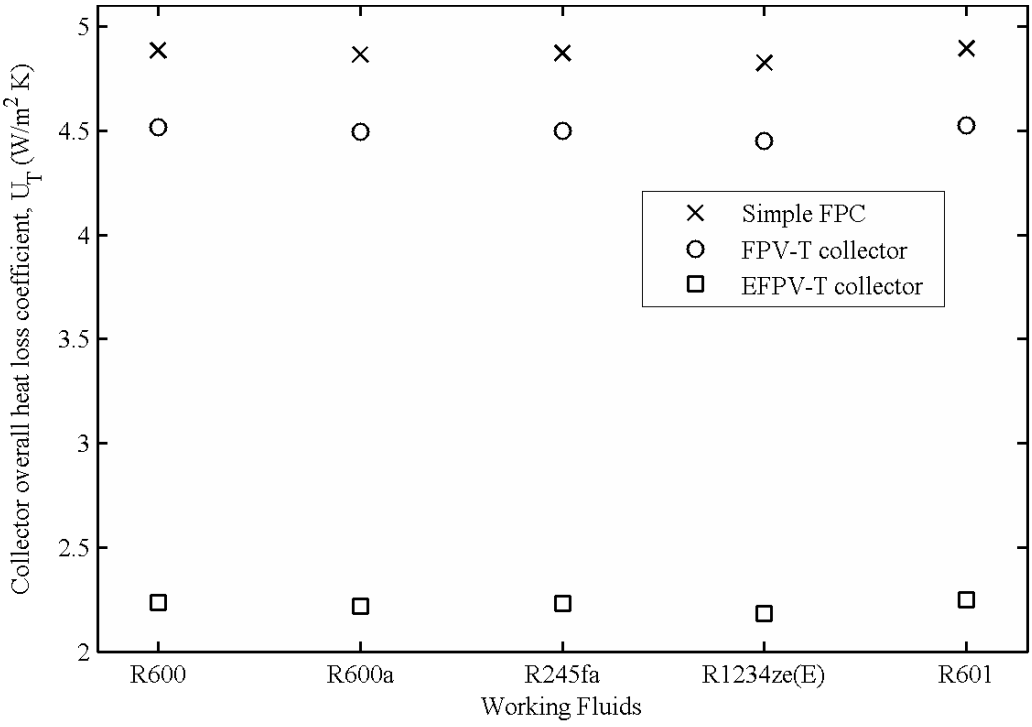

Figure 21 Collector overall heat loss coefficient for all working fluids under three different collector configurations

Figure 21 represents overall heat loss coefficient for all five working fluids, which is one of the most important factor in comparing the three different types of collector configurations. It can be seen that overall heat loss coefficient in EFPV-T collector configuration case is significantly low. It is because of the fact that in EFPV-T collector configuration case there is no air medium for natural convection to propagate from the absorber plate top, consequently reducing the collector's overall heat loss coefficient and enhances the collection efficiency as presented in Figure 19. It can also be observed from Figure 21 that overall heat loss coefficient has slightly reduced in case of FPV-T collector configuration but it hasn't helped improve the collector's performance and collector collection efficiency and heat absorbed is found to be the lowest for FPV-T configuration, as shown in Figure 19 and Figure 20 respectively. The reason behind this is that the reduction in overall heat loss coefficient is not as prominent as the negative effect of the drop in effective transmission-absorption product. It is due to the fact that a portion of the solar radiations is absorbed by the PV module bonded over the absorber plate, blocking the radiations from directly reaching the absorber plate and converts a portion of the energy into electricity depending on PV conversion efficiency.

R245fa and R600 respectively exhibit the highest and lowest collection efficiency of 61.27% and 58.58% at 1.5 pressure ratio under EFPV-T collector configuration, as shown in Figure 19. R245fa experienced a 12.44% increase in collection efficiency, from 48.83% in FPV-T configuration to 61.27% in EFPV-T configuration.

4.1.2 Net Work Output

Figure 23 displays the net work output of the system for five working fluids and under three collector configurations. Net work output of the system increases with increasing pressure ratio, as shown in Figure 23. It can be seen from Figure 23 that net work output first increases rapidly then slows down, with increasing pressure ratio. It can be explained by the fact that as the pressure ratio increases, fluid has to be pumped to a higher pressure consuming more input pump power and the working fluid's mass flow rate decreases to achieve the required outlet temperature (Figure 22). For R600 and R600a, in simple FPC and FPV-T configurations, net work output almost remains constant after peaking at pressure ratio 2.5. But in case of EFPV-T configuration,

working fluids exhibit an upward trend. The reason for this upward trend in EFPV-T configuration is that at the same pressure ratio more heat is absorbed in the collector which dominates the increase in pump work input and decrease in mass flow rate.

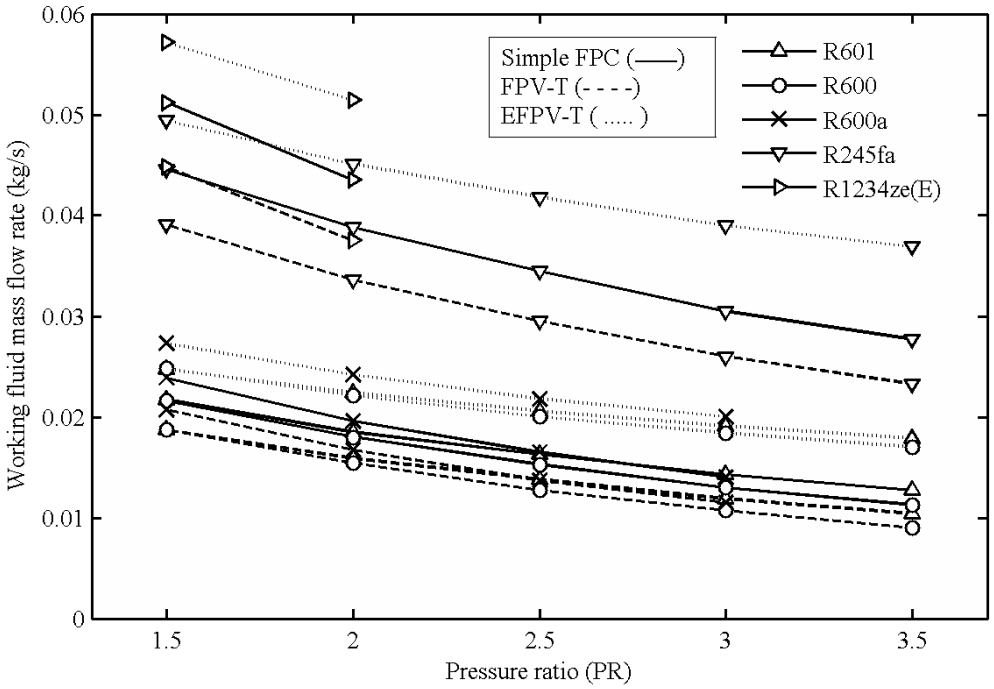

Figure 22 Working fluids mass flow rate vs PR

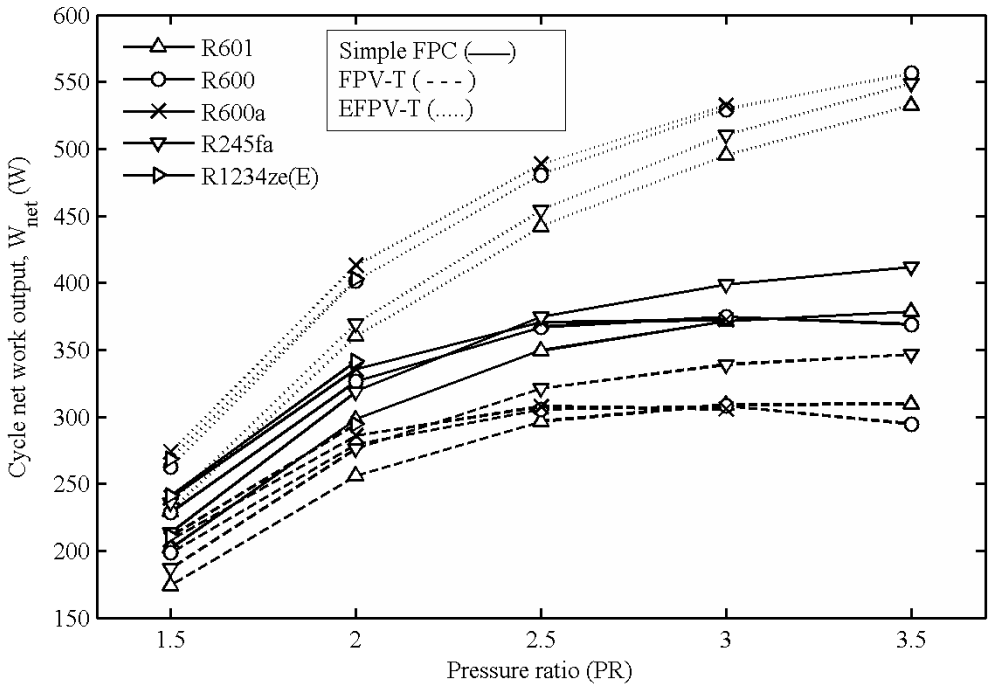

Figure 23 Cycle net work output under various pressure ratio points

It can also be observed from Figure 23 that at pressure ratio 3, net work output of R600, R600a and R245fa increased by 221.4W, 226.5W and 168.5W, respectively, from FPV-T to EFPV-T configuration. Thus, a significant improvement in net work output is achieved.

4.1.3 ORC Efficiency

Figure 24 displays the Rankine cycle efficiency versus pressure ratios for five working fluids. It can be observed that Rankine cycle efficiency increases with increasing pressure ratio. When pressure ratio increases the enthalpy drop between collector outlet to condenser inlet increases thus higher turbine output power is obtained consequently increasing the cycle efficiency.

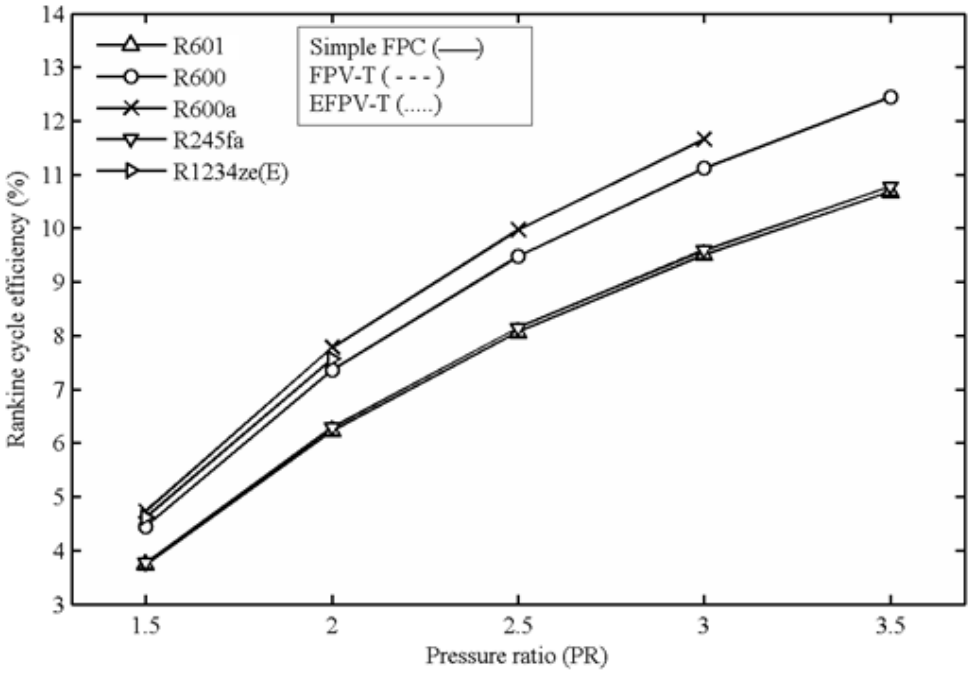

Figure 24 Rankine cycle efficiency versus pressure ratio

Results in Figure 24 also revealed that the ORC efficiency has not changed for all three types of collector configurations. This can be explained by the fact that in EFPV-T and FPV-T collector configurations, as the heat absorption in collector changes (increases in EFPV-T and decreases in FPV-T case) the corresponding turbine output also changes and the resulting ratio remains the same. The highest Rankine cycle efficiency is displayed by R600 ranged from 12.44% to 4.45% while R245fa displayed the lowest

cycle efficiency ranged from 10.78% to 3.77%. However, till pressure ratio 3 fluid R600a proves to be most efficient and recorded the highest cycle efficiency of 11.65%.

4.1.4 Overall Thermal Efficiency

Simulation results for overall thermal efficiency versus pressure ratio are represented in Figure 25. Overall thermal efficiency follows the same trend as net work output of the cycle. This behavior is due to the effect of net work output, shown in Figure 23, as input ($A_{col} \times I_s$) remain constant (behavior of net work output dictates the overall thermal efficiency).

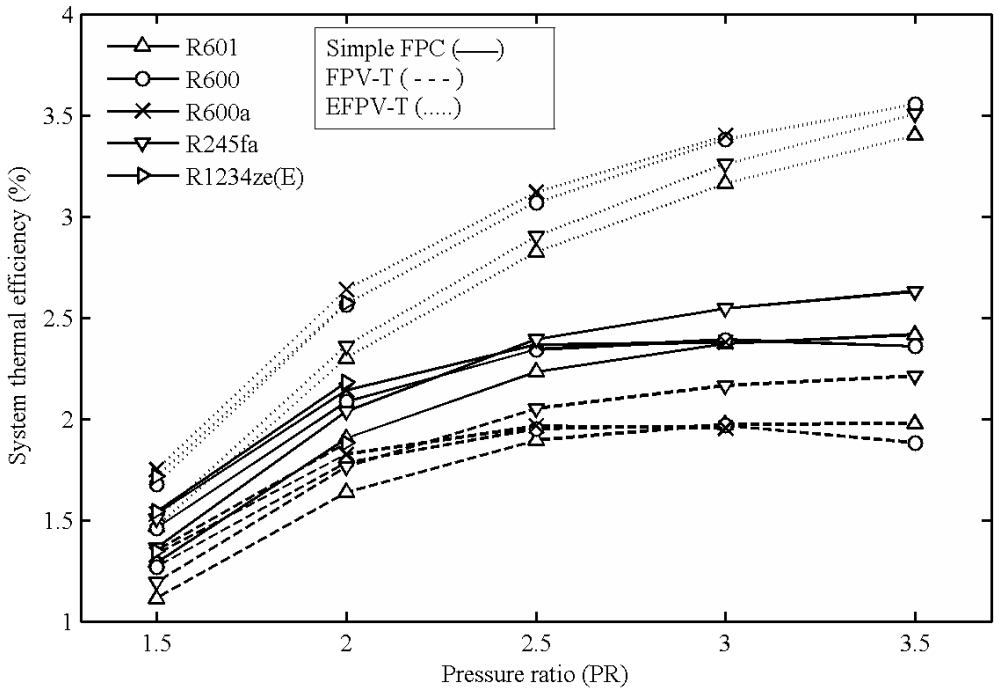

Figure 25 System's thermal efficiency versus various pressure ratios

Figure 25 shows that overall thermal efficiency is higher in EFPV-T case and R600 exhibits the highest efficiency of 3.55% at 3.5 pressure ratio. Comparing FPV-T and EFPV-T configurations, overall thermal efficiency of R600, R245fa and R600a increased by 1.67%, 1.29% and 1.45% respectively.

4.1.5 PV Electrical Efficiency

Another important component of the system is the PV module bonded over collector absorber plate. As the working fluid flows in the collector tubes its temperature rises

thus increasing the absorber plate temperature along the collector tube's length. Therefore, as the absorber plate temperature varies along the length of the collector tube, the PV electrical efficiency also changes. The absorber plate temperature and PV electrical efficiency, under increasing pressure ratio, are investigated at fluid's evaporation temperature. It can be observed from Figure 26 that PV electrical efficiency is decreasing with increasing cycle pressure ratio. It is because at higher pressure ratio fluid has to achieve a higher evaporation temperature hence a higher absorber plate temperature is observed, as apparent from Figure 27. Working fluid's evaporation temperatures at different pressure ratio points are presented in Figure 18.

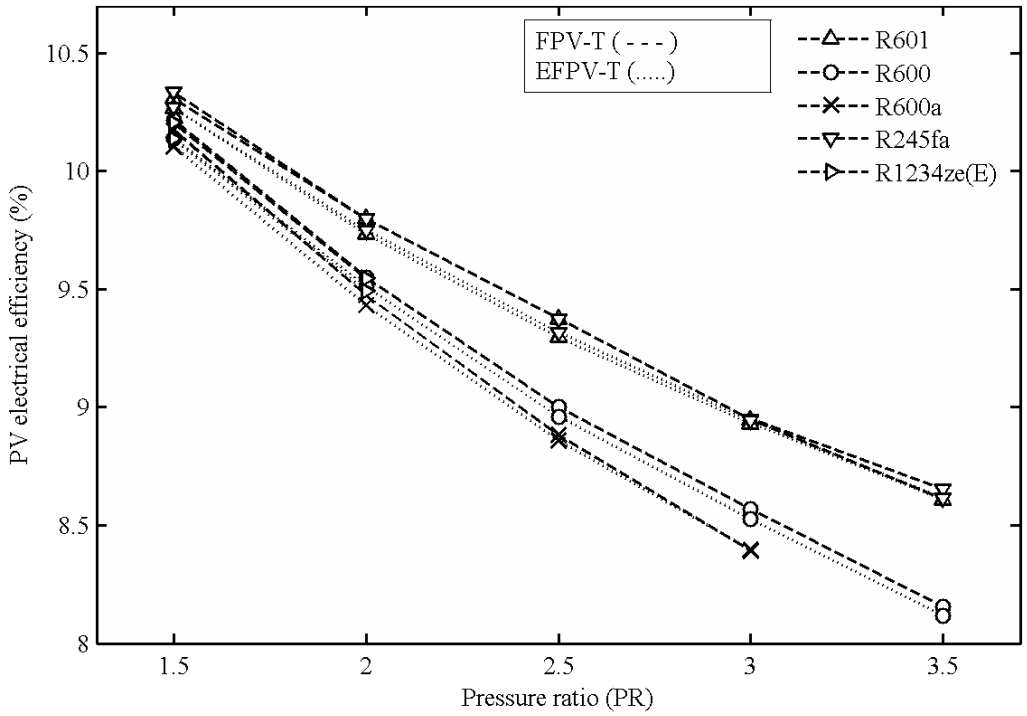

Figure 26 PV electrical efficiency with pressure ratios

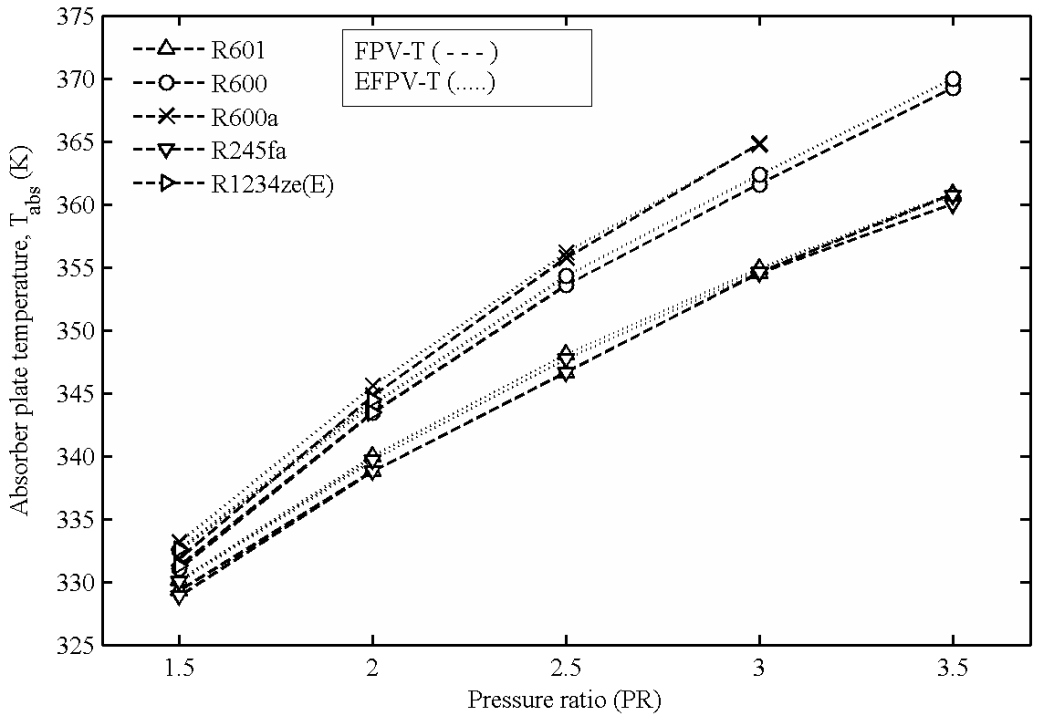

Figure 27 Absorber plate temperature with pressure ratios

A slight rise in absorber plate temperature can also be observed in case of EFPV-T collector configuration while PV electrical efficiency has slightly reduced. This rise in absorber temperature is not as significant as the reduction in heat loss component in EFPV-T configuration. It is because in EFPV-T configuration the mass flow rate of working fluid also increases, as presented in Figure 22, that takes away most of the heat from absorber and consequently the absorber plate temperature doesn't rise significantly. R245fa exhibits the highest PV electrical efficiency which varies from 10.33% to 8.65% in FPV-T configuration and 10.27% to 8.61% in EFPV-T configuration, respectively.

PV electrical efficiency and absorber plate temperature behavior have also been investigated along the length of the collector tube, as presented in Figure 28 and Figure 29 respectively. These results are obtained at the highest allowable pressure ratio that could be achieved by the working fluids, in the range of 1.5 - 3.5. R600, R601 and R245fa could achieve pressure ratio of 3.5 and the saturation temperatures at corresponding evaporation pressures are 361.91 K, 352.8 and 353.25 K, respectively. R600a and R1234ze(E) could achieve pressure ratios of 3 and 2. The

saturation temperatures for R600a and R1234ze(E) at the corresponding evaporation pressures and pressure ratios are 357.56 K and 337.66 K respectively. It can be observed from Figure 29 that absorber plate temperature initially tends to increase along the length of collector tube, reaches its peak (fluid achieved saturated liquid point), and then slightly drops and remain almost constant (fluid is in 2-phase flow). The drop in absorber plate temperature when fluid reaches 2-phase flow is because during phase change fluid's heat capacity is maximum which increases the heat removal factor thus decreasing the absorber plate temperature and it remains almost constant during the phase change process (fluid temperature is constant during phase change). Absorber temperature drops again when fluid enters the second collector (tube length, 56m), it is because the fluid enters the second collector at a higher temperature which reduces the heat gain.

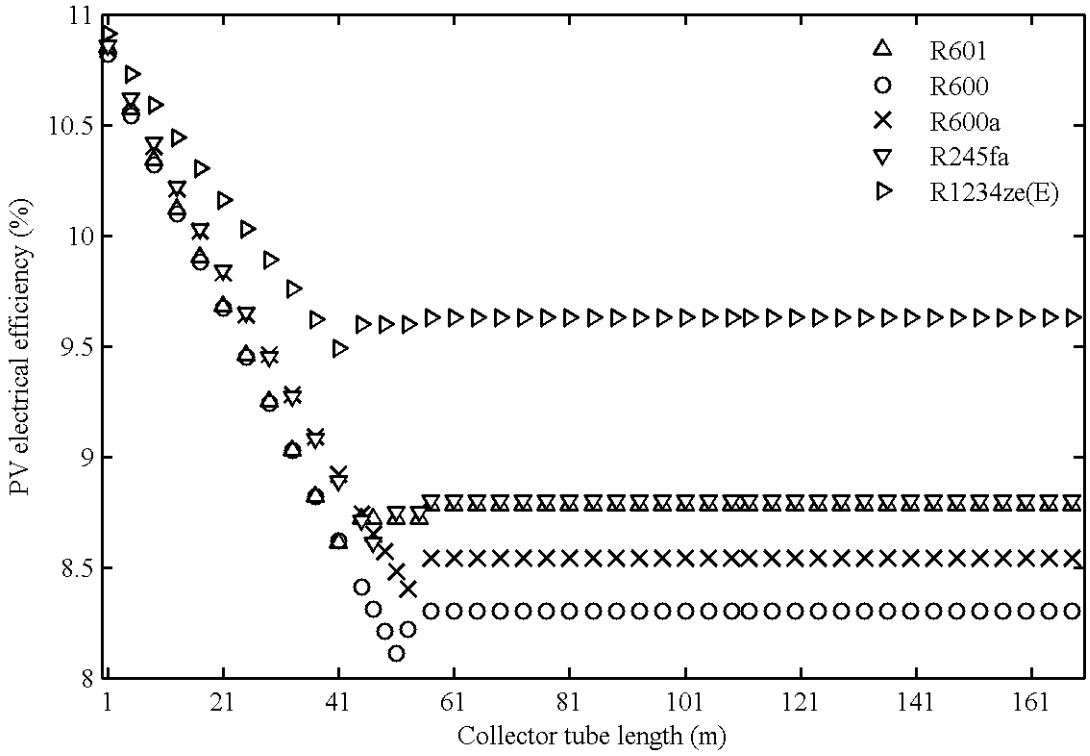

Figure 28 PV electrical efficiency variation along collector tube length for R601, R600 R600a R245fa and R1234ze(E)

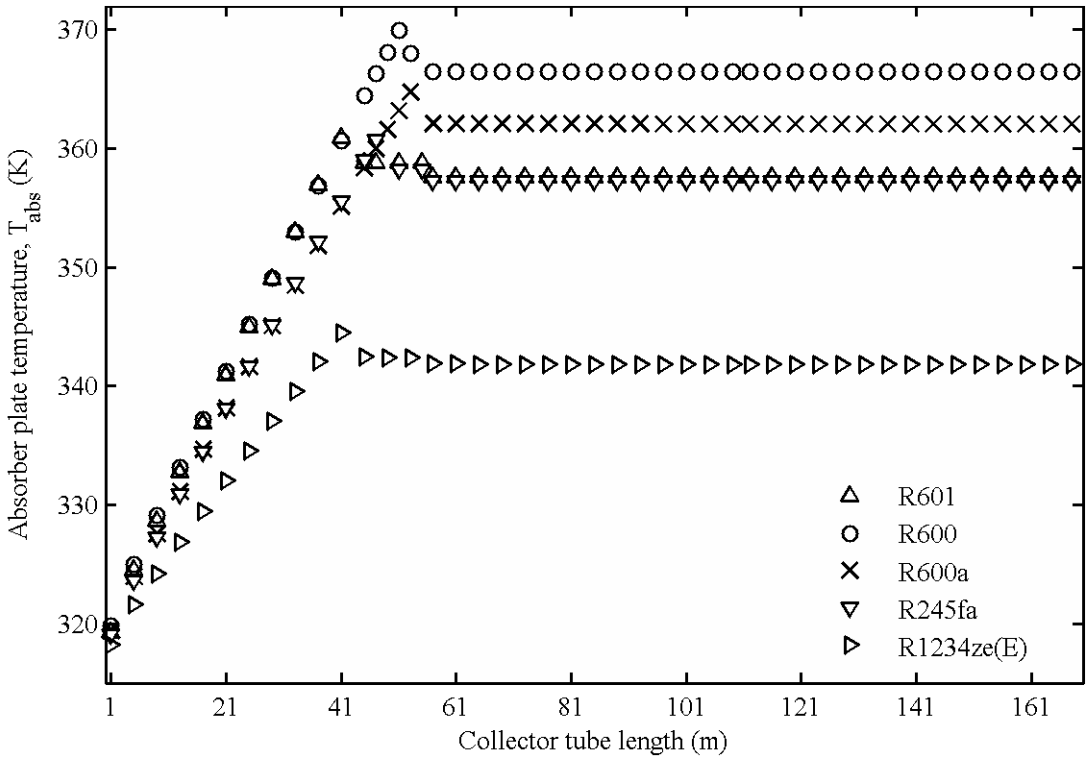

Figure 29 Absorber plate temperature variation along collector tube length for R601, R600, R600a, R245fa, and R1234ze(E)

As it can be seen from Figure 29, R600 exhibits the highest absorber temperature of 369.9 K at 51m tube length followed by R600a with absorber temperature of 364.8 K at 53m. The reason for the high absorber temperature is their high saturation temperatures, as mentioned earlier.

On the other hand, PV electrical efficiency is decreasing along the collector tube length, as shown in Figure 28. PV cells have experienced the lowest efficiency of 8.11% and 8.39%, respectively for R600 and R600a at collector tube length 51m and 53m. It can be seen from Figure 29 that although, R245fa is operating at high pressure ratio of 3.5 its saturation temperature is low and hence displays lower absorber temperature as compare to R600 and R600a.

4.1.6 System Overall Electrical Output

System overall power output per unit area for five working fluids and three different collector configurations is represented in Figure 30. In simple FPC configuration the electrical output is obtained only from the ORC expander and in Figure 30 it is

represented as net work output per unit area (solid line), and as the pressure ratio increases higher net work output is obtained. On the other hand, in FPV-T collector configuration system overall electrical output per unit area is decreasing with increasing pressure ratio and it represents combined electrical output of both PV and ORC expander. The increase in ORC expander output is not as significant as the drop in PV efficiency with increasing pressure ratio that's why system overall electrical output curve in FPV-T configuration shows a decreasing trend. However, in EFPV-T configuration case system overall electrical output showed an increasing trend till 2.5 pressure ratio and almost remains constant afterwards.

Fluid R245fa obtained the highest system overall electrical output at 3.5 pressure ratio which exhibited an increase of 9.48 W/m^2 from 67.33 W/m^2 in FPV-T configuration to 76.81 W/m^2 in EFPV-T configuration case, as displayed in Figure 30.

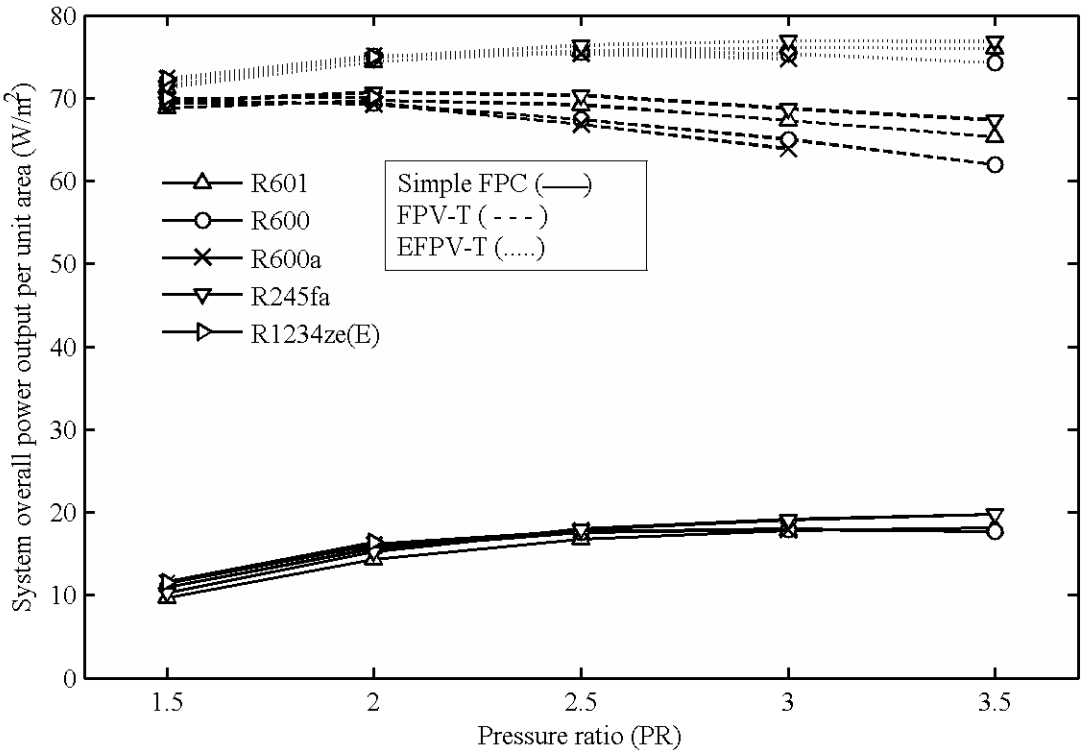

Figure 30 System overall power output per unit area

4.1.7 System Overall Electrical Efficiency

System overall electrical efficiency is displayed in Figure 31 for FPV-T and EFPV-T collector configurations. EFPV-T collector configuration exhibits higher system overall

electrical efficiency as compare to FPV-T configuration. It can be observed from Figure 31 that at PR 2.5 and above R245fa displays the highest overall electrical efficiency under EFPV-T configuration and displayed 8.24% of system overall electrical efficiency at 3.5 pressure ratio.

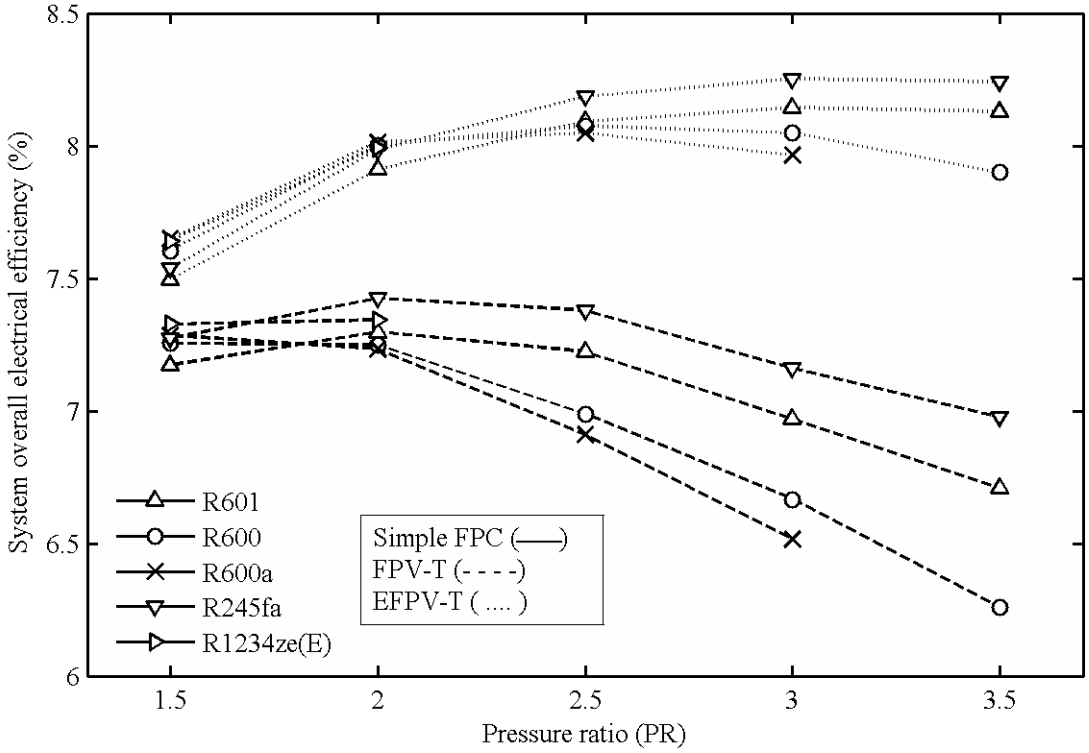

Figure 31 System overall electrical efficiency

The reason for better overall performance of working fluid R245fa is due to the fact that at all pressure ratios R245fa exhibits lower evaporation temperature (Figure 18) as compare to other fluids which results in lower absorber plate temperature (Figure 27) and PV cells perform more efficiently, consequently higher overall output is achieved.

Chapter 5

Conclusion and Recommendations

5.1 Conclusion

A mathematical model for saturated solar ORC system was developed, utilizing solar collector as a direct vapor generator, to assess the performance of the system under different pressure ratios (1.5-3.5) and three different collector configurations. MATLAB software was used to perform the simulations.

- It was observed that in case of FPV-T collector configuration, solar collector's performance dropped. The PV module bonded over the absorber plate, absorbed a portion of the incoming solar radiation hence decreased the useful heat gain of working fluid in collector tubes. Minimum collector efficiency was observed to be 24.09% at 3.5 pressure ratio for R600 in FPV-T collector configuration. In EFPV-T collector configuration, solar collector's performance improved significantly and maximum efficiency of 61.27% was found at pressure ratio 1.5. The lower heat loss coefficient in the proposed system resulted in the improvement of system's performance.

- Performance of ORC system is directly related to the solar collector behavior. Therefore, improvement in ORC system thermal efficiency was observed in EFPV-T collector configuration and in FPV-T configuration thermal efficiency dropped. Results showed that at pressure ratio 3.5 R600 achieved maximum system thermal efficiency of 3.55% in EFPVT collector configuration. Rankine cycle efficiency was found to be not effected in changing the collector configuration. R600 obtained maximum Rankine cycle efficiency of 12.44% and net power output of 556.4W at 3.5 pressure ratio.

- PV electrical efficiency is found to be decreasing with increasing pressure ratio because absorber plate temperature increases. Simulation results revealed that PV electrical efficiency also decreases along the length of the collector and is minimum at saturated liquid point where fluid starts to change phase. PV

performs more efficiently when ORC is operated at lower evaporation temperature. A slight reduction in PV efficiency in EFPV-T collector configuration has also been observed.

- Simulation results revealed that the system's overall performance has significantly improved in EFPV-T collector configuration. The decreasing trend of PV electrical efficiency with increasing pressure ratio and the slight reduction in PV electrical efficiency under EFPV-T configuration have been offset by the increase in expander output under EFPV-T collector configuration.

- Simulation results revealed that fluids with low boiling point require higher evaporating pressure that will limit its use in domestic flat plate solar collector used as evaporators. It was also found that evaporating temperature is an important parameter in PVT collectors because it dictates the absorber temperature consequently affecting the PV performance. Fluid with low evaporating temperature at high pressure ratio would be a suitable candidate as far as PV performance is concerned in a PVT collector. Results show that at pressure ratio 3.5 R601 exhibited lower saturation temperature as compare to R600 and R245fa.

5.2 Recommendations

In order to broaden the scope of current study, the photo-thermal properties of the EFPV-T collector should be investigated at higher temperatures along with different types of solar cells available today and appropriate cell should be determined. Furthermore, the working fluids selected in this study should be investigated at higher cycle temperatures and more fluids that are available in literature should be included in the analysis.

5.3 Future work

The proposed EFPV-T collector will be designed and fabricated based on the modeling and simulation results obtained in this study. This demo unit will be installed at USPCASE, NUST Islamabad. Once the fabrication and installation phase is completed, we will be able to get the real time performance data for the collector. The practical implementation of this study will prove the effectiveness of the system and will help open more doors for research in the system fabrication, cost analysis and lifetime stability.

Performance Evaluation of an Evacuated Flat Plate Photovoltaic-Thermal (PVT) Collector for Heat and Electricity

Izaz Ahmad Qureshi
U.S.-Pakistan Centre for Advanced Studies in Energy
National University of Sciences and Technology
Islamabad, Pakistan
17eseizaz@uspcase.nust.edu.pk

Adeel Waqas
U.S.-Pakistan Centre for Advanced Studies in Energy
National University of Sciences and Technology
Islamabad, Pakistan
adeel@casen.nust.edu.pk

***Abstract*— The photovoltaic (PV) systems produce heat and electricity at the same time. Heat produced by conventional PV systems is of low-grade nature that cannot be used efficiently in high temperature application. In this article a novel PV thermal air collector has been worked out that can produce heat of high-grade nature as well as electricity. To obtain high temperature vacuum has been created between the solar cells and glass glazing that will reduce the thermal loss. Currently, in this work, a mathematical model is presented for single glazed evacuated flat plate photovoltaic-thermal (EFPVT) air collector to investigate its performance under different working conditions. The model is established on heat balance equations constructed for each component of the EFPVT air collector, considering a steady state heat transfer. MATLAB software is used to develop the computer code for the heat balance model and to run the iterative simulations. Simulations are performed at different mass flow rates (0.001-0.08 kg/s), collector length (1-10 m) and different configurations (evacuated/non-evacuated, with PV lamination and without PV lamination). The results indicate that thermal efficiency for EFPVT collector is higher and achieved higher outlet air temperature. A slight reduction in PV electrical efficiency is also observed due to rise in absorber temperature, in EFPVT collector case as compared to conventional non-evacuated configuration. The proposed mathematical model is suitable for steady state simulation and can successfully predict the system's electrical and thermal performance, in good conformity with the literature.**

Keywords—Renewable energy, Photovoltaic-thermal, Evacuated flat plate collector, Mathematical modeling, Performance analysis

I. INTRODUCTION

Fossil fuel reserves are depleting day by day and the world is in transition towards green and clean energy resources. One abundantly available renewable energy resource is solar energy. Photovoltaic (PV) systems are the most popular solar energy technology available in the market. PV systems work efficiently at low temperatures, however, during the operation its temperature rises rapidly which adversely affects the efficiency of the system[1]. Photovoltaic-thermal (PVT) systems provide a possible solution to this problem. Flat plate photovoltaic-thermal (FPVT) collector is one such practical system. In FPVT collector glass-glass (GG) or glass-tedlar (GT) PV module is bonded to the top of the collector's absorber and working fluid flow in the ducts attached below the absorber plate, removing the thermal energy and heat from the PV module, lowering module's temperature[2].

Air based PVT collector system performance for four different configurations were studied numerically and experimentally for Iraq climate conditions by [3]. A slight rise in the PV efficiency, with increasing working fluid mass flow rate, was observed and a double duct with single pass collector model was found to have the highest combined efficiency. In another study conducted by [4], four different PV module configurations were analyzed. It was reported that GG PV modules are best suitable for PVT systems exhibiting higher outlet air temperature and electrical efficiency. A mathematical model for a glazed PVT system was presented by [5] and the results were validated with experimental data. It was observed that electricity production of PVT collector was lower compared to a conventional PV system due to irradiation loss from the glazing but overall performance was higher because PVT system also produces thermal energy at the same time. Single and double glazing air type PVT collector was analyzed under transient condition for Delhi climate. An increase in system efficiency from 38% to 60% was observed with increasing working fluid mass flow rate from 0.007 kg/m^{2}s to 0.04 kg/m^{2}s, although at higher mass flow rates the efficiency increase is small [6].

FPVT collectors encounter convection heat loss from absorber plate to top glazing due to natural convective heat transfer between the two flat surfaces. Performance of FPVT collector can be enhanced by evacuating the air between top glazing and absorber plate hence lowering the internal pressure that will minimize the convection losses; such collectors are called evacuated flat plate photovoltaic-thermal (EFPVT) collectors. Optimal design for a simple evacuated flat plate collector was investigated to predict improvements in performance and then a comparative analysis was performed with other solar energy systems. It was reported that the system efficiency was improved by creating vacuum and heat loss coefficient was reduced to 3.7 W/m^{2}K [7]. Evacuated flat plate collectors exhibit higher thermal efficiencies than evacuated tube or flat plate collectors and can achieve efficiency of 62% at steam temperature of 100˚C [7][8].

FPVT systems and simple evacuated flat plate collectors have been extensively investigated in literature. In this work, both of these technologies are combined to introduce a novel concept of evacuated flat plate photovoltaic-thermal (EFPVT) collector. A detailed numerical model of an EFPVT collector has been developed and the algorithm is implemented using MATLAB software. Simulation study is conducted to investigate the collector's thermal efficiency and outlet temperature, and how this novel model would affect the electrical efficiency of PV module along the collector tube length and under different working fluid mass flow rates.

978-1-7281-5404-6/19/$31.00 ©2019 IEEE

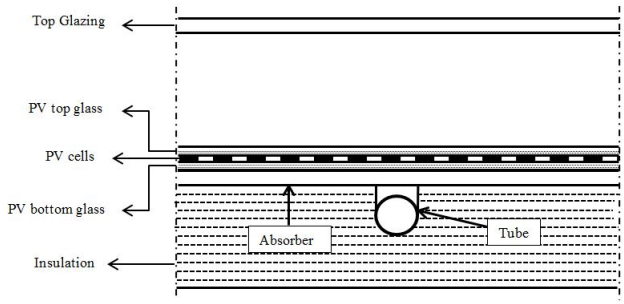

Fig. 1. EFPVT air collector with single glazing: cross-section view

II. Collector Specifications

In Fig. 1, a schematic cross-section view across a single tube of an EFPVT air collector is presented. It consists of a top glazing, glass-glass PV (GG PV) module, absorber plate, tube and insulation at the back of the collector. Top glazing with 0.003 m thickness is used to reduce convection and radiation losses. GG PV module is bonded on the surface of the absorber plate. The gap between the top glazing and GG PV module is 0.025 m, and air in the gap is evacuated to eliminate the natural convective heat transfer. Working fluid, air, is circulated in the copper tubes where it gains heat from the absorber. The copper tubes are arranged at equal spacing along the width of the absorber plate. Insulation is bonded at the rear end and edges of the collector to reduce the conduction loss.

TABLE I. Collector Specifications

Tube outer-diameter (m)	0.01
Tube inner-diameter (m)	0.008
Single unit area (m^2)	1
Thermal conductivity of absorber plate (W/m-K)	50
Thermal conductivity of tubes (W/m-K)	400
Thermal conductivity of insulation (W/m-K)	0.04
Absorber plate thickness (m)	0.002
Glass-glass PV module thickness (m)	0.0063
Insulation thickness (m)	0.025

III. Simulation Model

A simulation model is developed, based on energy balance equations constructed for each component of the EFPVT air collector, a cross-section schematic of which is depicted in Fig. 1. Energy balance analysis is performed under the following assumptions:

- Steady-state condition.
- Heat transfer is in one direction.
- Edge losses from collector are negligible.
- EVA transmissivity is 100%.
- Radiative and thermal properties of top glazing, GG PV module and absorber plate are constant independent of temperature.
- No heat is conducted from the absorber plate to back insulation; heat is transferred completely to the copper tubes.
- Temperature of all the components of the system varies along the direction of the airflow in tubes.
- Heat capacity effects for all the components of the system are negligible.

The EFPVT air collector is divided into different components (Top glazing, PV front glass & bottom glass, PV cells, absorber plate, tubes, fluid, and insulation) for thermal analysis. To perform the analysis, nine energy balance equations are developed and can be written as follows:

A. Top Glazing

In Equation(1) below, fraction of total solar insolation (I_s) absorbed by top glazing ($I_s\alpha_{GL}A_{GL}$) and radiation heat transfer to the top glazing (GL) from the PV module front glass (FG), is equal to the heat loss from top glazing to the environment through external convection and radiation. This equation is for evacuated configuration (EFPVT), as there is no natural convective heat exchange between top glazing and front glass of the PV module. For non-evacuated configuration, "($h_{3a} A_G (T_{FG} - T_{GL})$" is added to the left hand side of the equation, where "h_{3a}" is natural convective heat transfer coefficient between two flat parallel surfaces (FG of PV module and top glazing).

$$I_s\alpha_{GL}A_{GL} + h_3A_{GL}(T_{FG} - T_{GL}) = h_1A_{GL}(T_{GL} - T_{amb}) + h_2A_{GL}(T_{GL} - T_{sky}) \quad (1)$$

Where:

$$h_1 = 2.8 + 3\times w \text{ [9]} \quad (2)$$

$$h_2 = F\ 4\ \varepsilon_{GL}\sigma_{stf}\ [(T_{GL} + T_{sky})/2]^3 \quad (3)$$

$$h_3 = [\sigma_{stf}\ (T^2_{FG} + T^2_{GL})(T_{FG} + T_{GL})]/[1/\varepsilon_{FG} + 1/\varepsilon_{GL} - 1] \text{[9]} \quad (4)$$

$$T_{sky} = 0.0522\times(T_{amb})^{1.5} + 2.62\times N \text{ [10]} \quad (5)$$

h_1 and h_2 are respectively the external convective and radiative coefficients of top glazing to the environment (W/m^2K); h_3 - natural radiative heat coefficient between FG of PV module and top glazing (W/m^2K); w - wind velocity (m/s); th - thickness (m); α_{GL} and ε_{GL} are respectively the absorptivity and emissivity of top glazing; T_{GL}, T_{FG}, T_{amb}, and T_{sky} are respectively the temperatures of top glazing, FG of PV module, ambient and sky; N – sky cloud coverage (for clear sky, N = 0); $A_{GL} = A_{FG} = A_{BG} = A_{abs}$, Areas ($m^2$).

B. PV Front Glass:

Solar radiation after being transmitted through glazing (τ_{GL}) strikes the FG of PV module and a fraction of it is absorbed ($I_s\ (\tau_{GL}\alpha_{FG})\ A_{FG}$). Conduction heat exchange (h_4) occurs between PV module cells and FG. For non-evacuated configuration, ($h_{3a} A_G (T_{FG} - T_{GL})$) is added to the right hand side of (6).

$$I_s(\tau_{GL}\alpha_{FG})A_{FG} + h_4A_{FG}(T_{PV} - T_{FG}) = h_3A_{FG}(T_{FG} - T_{GL}) \quad (6)$$

Where:

$$h_4 = K_{FG} / th_{FG} \quad (7)$$

h_4 - conductive heat transfer coefficient of PV module FG (W/m^2K), related to its thermal conductivity (K_{FG}) and thickness (th_{FG}); τ_{GL} and α_{FG} are respectively the transmissivity of top glazing and absorptivity of PV module FG; T_{PV} - PV cell temperature (K).

C. PV Cells

PV module cells absorb (α_{PV}), 85% of the incident light[11]. Depending on its efficiency (η_{PV} =12%) a small portion of incident light is converted into electrical energy and the rest is lost as heat. 85% packing factor (PF) of PV module cells is considered. Thermal energy generated in PV module cells is conducted to top and bottom glass of the module.

$$I_s (\tau_{GL}\, \tau_{FG}\, \alpha_{PV})\, A_{PV}PF - \eta_{PV}\, I_s\, A_{PV}PF = h_4 A_{PV}PF\, (T_{PV} - T_{FG}) + h_5 A_{PV}PF\, (T_{PV} - T_{BG}) \quad (8)$$

Where:

$$h_5 = K_{PV} / th_{PV} \quad (9)$$

h_5 - PV cells conductive heat transfer coefficient (W/m^2K), related to its thermal conductivity (K_{PV}) and thickness (th_{PV}); η_{PV} and α_{PV} are respectively the PV efficiency and absorptivity; $A_{PV}PF$ - used to calculate the PV cell area, depends on PV module's packing factor (PF); T_{BG} - PV module bottom glass (BG) temperature (K).

D. PV Bottom Glass

A portion of solar radiation is directly transmitted from FG to BG of PV module through vacant space between the adjacent cells, a fraction of it is absorbed by BG "$I_s (\tau_{GL}\, \tau_{FG}\, \alpha_{BG})\, A_{BG}\, (1 - PF)$" and the rest is transmitted to the absorber plate. BG is thermally bonded to the absorber plate, so heat transfer from PV cells to absorber depends on the BG conductivity.

$$I_s (\tau_{GL}\, \tau_{FG}\, \alpha_{BG})\, A_{BG}\, (1 - PF) + h_5 A_{PV}PF\, (T_{PV} - T_{BG}) = h_6 A_{BG}\, (T_{BG} - T_{abs}) \quad (10)$$

Where:

$$h_6 = K_{abs} / th_{abs} \quad (11)$$

h_6 - absorber plate's conductive heat transfer coefficient (W/m^2K), related to its thermal conductivity (K_{abs}) and thickness (th_{abs}); τ_{FG} and α_{BG} are respectively the transmissivity and absorptivity of FG and BG of PV module; T_{abs} - absorber plate temperature (K).

E. Absorber plate

Solar radiation transmitted through BG is absorbed by absorber plate "$I_s\, (\tau_{GL}\, \tau_{FG}\, \tau_{BG}\, \alpha_{abs})\, A_{abs}\, (1 - PF)$" and is converted to thermal energy, rest of the thermal energy is received through conduction from BG. From absorber plate heat is conducted to the attached copper tubes.

$$I_s (\tau_{GL}\, \tau_{FG}\, \tau_{BG}\, \alpha_{abs})\, A_{abs}\, (1 - PF) + h_6 A_{BG}\, (T_{BG} - T_{abs}) = h_7 A_{abs\text{-}tube}\, (T_{abs} - T_{tube}) \quad (12)$$

Where:

$$h_7 = K_{tube} / th_{tube} \quad (13)$$

$$A_{abs\text{-}tube} = n\, (D_o\, L) \quad (14)$$

h_7 - conductive heat transfer coefficient in tube (W/m^2K); τ_{BG} and α_{abs} are respectively the transmissivity of BG and absorptivity of absorber plate; $A_{abs\text{-}tube}$ - absorber plate to tube area (m^2); D_o - outer diameter of tube (m); L - length of single tube element; T_{tube} - tube temperature (K) ; n - number of copper tubes.

F. Tubes

Heat conducted from absorber plate to copper tubes is transferred to the working fluid inside and attached thermal insulation at the back.

$$h_7 A_{abs\text{-}tube}\, (T_{abs} - T_{tube}) = h_{8a}\, A_{tube\text{-}f}\, (T_{tube} - T_{mf}) + h_{8b}\, A_{tube\text{-}ins}\, (T_{tube} - T_{ins}) \quad (15)$$

Where:

$$h_{8a} = (Nu_f \times K_f) / D_{in} \quad (16)$$

$$h_{8b} = K_{ins} / (\, th_{ins} / 2) \quad (17)$$

$$A_{tube\text{-}f} = n\, (\pi D_{in}\, L) \quad (18)$$

$$A_{tube\text{-}ins} = n\, (D_o\, L) \quad (19)$$

For fully developed laminar flow ($Re < 2300$):

$$Nu_f = 4.36 \quad (20)$$

For fully developed turbulent flow:

$$Nu_f = 0.023 \times Re^{0.8} \times Pr^{0.4}\, [12] \quad (21)$$

h_{8a} - forced convective heat transfer coefficient for working fluid in tubes (W/m^2K), depends on Nusselt (Nu) number, fluid conductivity (K_f) and tube inner diameter (D_{in}); Pr – Prandtl number; Re – Reynolds number; h_{8b} is conductive heat transfer coefficient for back insulation (W/m^2K); $A_{tube\text{-}f}$ - tube to working fluid area (m^2); K_{ins} and th_{ins} are the thermal conductivity and thickness of back insulation, respectively.

G. Fluid in Tubes

The energy transferred to the fluid in tubes is equal to the thermal energy coming out from that element, and it then enters the adjacent element with higher inlet temperature.

$$h_{8a}\, A_{tube\text{-}f}\, (T_{tube} - T_{mf}) = 2\, m_f\, C_f\, (T_{mf} - T_{in}) \quad (22)$$

Where:

$$T_{mf} = (T_{out} + T_{in})/2 \quad (23)$$

C_f (kJ/kg K) and m_f (kg/s) are respectively the heat capacity and mass flow rate of air flowing in tubes; T_{mf} - mean fluid temperature in single element that is under analysis; T_{in} – inlet temperature of fluid (K); T_{out} - outlet temperature of fluid (K).

H. Back Insulation

Thermal energy conducted to the back insulation from tubes, is dissipated to the environment through external convection, while radiation from back is negligible.

$$h_{8b}\, A_{tube\text{ - }ins}\, (T_{tube} - T_{ins}) = h_9\, A_{ins}\, (T_{ins} - T_{amb}) \qquad (24)$$

Where "$h_9 = [\ (th_{ins} / 2)/K_{ins} + 1/(2.8 + 3w)\ ]^{-1}$" includes both conductive and convective heat transfer coefficients from back insulation; T_{ins} - back insulation temperature (K).

For performance analysis, electrical and thermal parameters of the system are investigated. Thermal efficiency of the system can be calculated with the following equation:

$$\eta_{th} = [\ m_f\, C_f\, (T_{out} - T_{in})] \,/(\, I_s\, A_c) \qquad (25)$$

To compute the PV module electrical efficiency, following equation is used:

$$\eta_{PV} = \eta_n\, [1 - \beta\, (T_{PV} - T_{ref})]\ [13] \qquad (26)$$

where η_n is PV nominal electrical efficiency at reference temperature (T_{ref}) . β is the PV cell temperature coefficient ($^{\circ}C^{-1}$).

To study the overall performance of the system, another parameter of overall system efficiency (η_o) is used[14]:

$$\eta_o = \eta_{th} + \eta_{PV} \qquad (27)$$

IV. Iteration Procedure

For numerical analysis collector is divided into 20 elements, along the length of a single copper tube, each of length 0.5 m. Width of each element is constant 0.03m, along the collector length. Temperature of different components in each element is assumed to be uniform while the air temperature in tube increases along the length, hence mean air temperature is calculated in each element, (23). Utilizing iterative procedure, temperature of top glazing, FG, PV cells, BG, absorber plate, tube, insulation, and mean air temperature are calculated. MATLAB computer software is used to run the program developed for the iterative process. COOLPROP program [15] is linked with MATLAB to find the thermal conductivity (K_f) and heat capacity (C_f) of air that changes with the temperature rise.

Initially, all components and mean air temperature of the first element are assumed to be equal to ambient temperature, (T_{amb} = 302 K). The program starts with the first element *i=1* and takes the initially assumed temperature values. Iteration process is initiated and the program calculates the heat loss and heat transfer coefficients and imports the thermo-physical properties of air from COOLPROP program. Three matrices [A], [B] and [C] are set-up and new temperatures are calculated. If the difference between corresponding new and previous temperature values is less than or equal to the convergence criterion *e=0.001˚C,* the iteration will end and new temperatures will

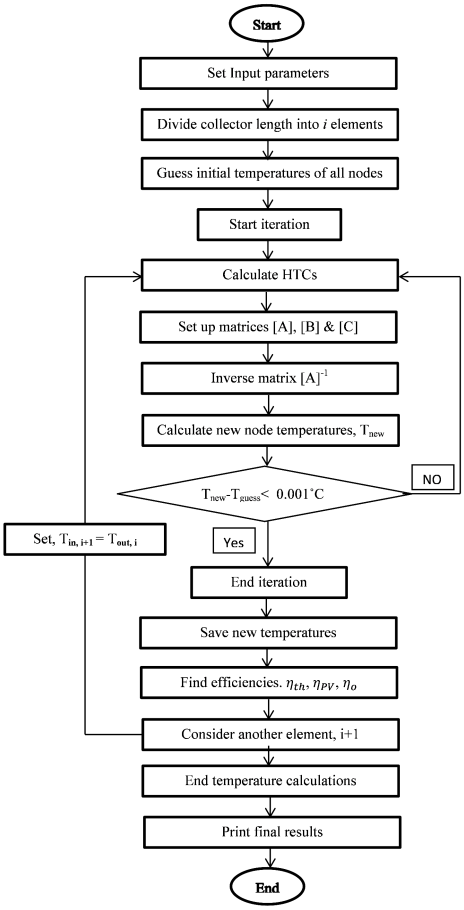

Fig. 2. Simulation procedure flow chart

be saved for that element. Thermal, electrical and system overall efficiencies, and air outlet temperature are calculated at the end of the iteration. For another loop, the program increases the length of the collector and adds another element *i+1*, and repeats the same procedure. When the number of element reaches *i=20*, means the length of collector is 10 m, the program will end and prints final results and graphs.

V. Results and Discussion

The simulations are performed at 700 W/m^2 of solar insolation, 302 K ambient and air inlet temperature and 1 m/s wind velocity. GG PV module of 12% cell efficiency and 85% packing factor is bonded to the absorber plate top surface. Four different collector configurations are analyzed, to study its performance under different working conditions of increasing air mass flow rate and collector tube length. Four cases are defined as follows:

- Case 1. Non-evacuated FPC without PV module
- Case 2. Non-evacuated FPC with GG PV module
- Case 3. Evacuated FPC with GG PV module
- Case 4. Evacuated FPC without PV module

Graphs in Fig. 3 and Fig. 4 show the effect of air mass

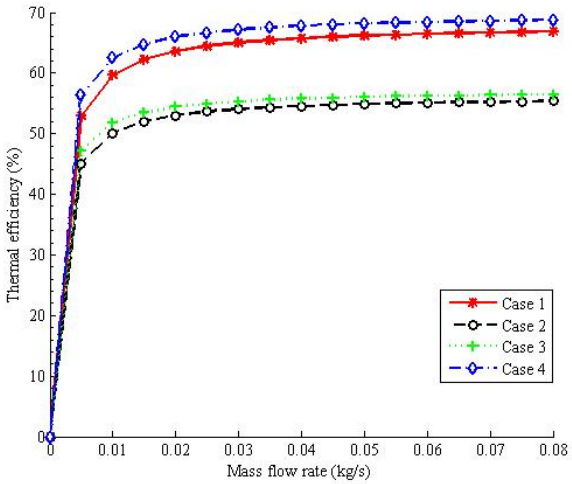

Fig. 3. Effect of working fluid mass flow rate on collector thermal efficiency

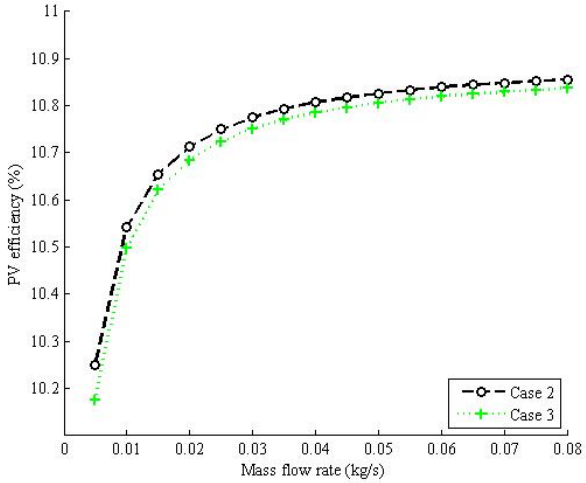

Fig. 4. Effect of working fluid mass flow rate on PV electrical efficiency

flow rate *(m_f)* on thermal efficiency (η_{th}) and PV electrical efficiency (η_{PV}) of the collector in 4 different cases. Both the efficiencies, thermal and electrical, increase with increasing mass flow rate of air from 0.005 kg/s to 0.08 kg/s, and curves tend to saturate around 0.04 kg/s. Case 4 and 2 exhibit the highest and lowest thermal efficiencies of 68.75% and 55.35% at mass flow rate of 0.08 kg/s, respectively as shown in Fig. 3. Observing the evacuated configurations, Case 3 and Case 4, an increase in thermal efficiency of 1.2% and 2.08% is shown from the corresponding non-evacuated configurations (Case 2 and 1) respectively, at 0.04 kg/s as presented in Fig. 3.

In case of non-evacuated configuration the top heat loss coefficient of the collector is found to be 5.35 W/m^2 K at 0.04 kg/s mass flow rate, which is reduced to 4.11 W/m^2 K for evacuated configuration. This reduction in heat loss coefficient results in enhancement of thermal efficiency observed in Case 3 & 4 as shown in Fig. 3, which are evacuated configurations. In Fig. 4, PV efficiency has slightly dropped in Case 3 that is due to GG PV module's temperature rise because of reduced thermal loss from the top of the module.

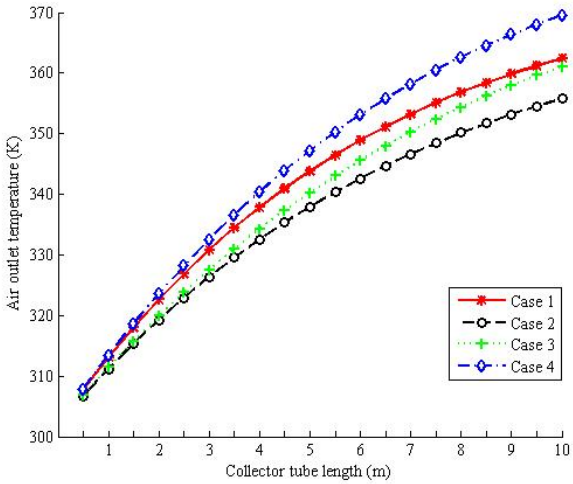

Fig. 5. Variation of outlet air temperature along collector tube length

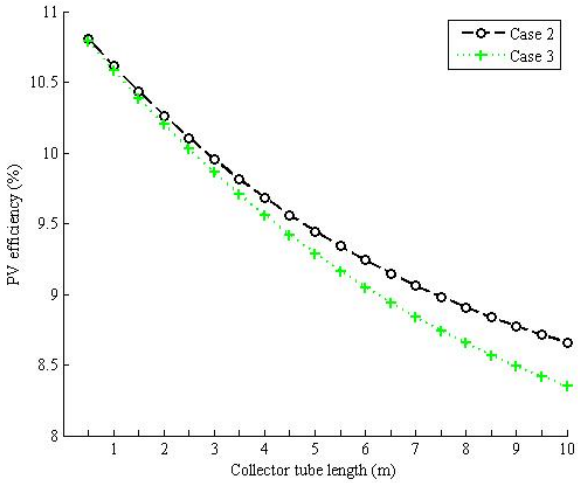

Fig. 6. PV electrical efficiency along collector tube length

The graph in Fig. 5 presents the variation of outlet air temperature with collector tube length. Air temperature is observed to be increasing along the collector tube length. Highest outlet air temperature of 369.5 K is achieved in Case 4. Evacuated configurations Case 3 and 4 observed 5.3 K and 7.1 K rise in outlet air temperature from the non-evacuated configurations of Case 2 and 1, as shown in Fig. 5.

It can be seen from Fig. 6 that PV efficiency decreases along the length of collector. It can be explained by the fact that as the air flows in the tube along the length of collector it gains thermal energy and its temperature rises, which in-turn rises the temperature of absorber plate and attached PV module. Consequently, this rise in temperature of PV module results in drop of PV efficiency. This drop in PV efficiency is more prominent in evacuated configuration (Case 3) because of no convective heat transfer from the PV module's top as mentioned earlier, and it varies from 10.79% to 8.35% along collector length, as apparent from Fig. 6.

System overall efficiency is plotted as a function of mass flow rate in Fig. 7. Comparing the system overall efficiency for evacuated and non-evacuated configurations, Case 3 and

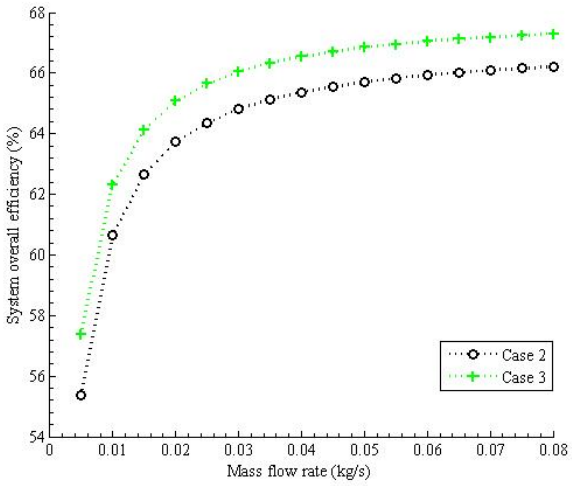

Fig. 7. System overall efficiency versus working fluid mass flow rate

Case 2, at mass flow rate 0.04 kg/s an increase of 1.18% can be observed, as depicted in Fig. 7. Case 3 achieved an overall efficiency of 67.3% at 0.08 kg/s. In EFPVT case, the increase in thermal efficiency offsets the drop in PV efficiency hence overall system efficiency improves.

VI. Conclusion

A mathematical model based on heat balance equations has been presented, for air heating evacuated flat plate photovoltaic-thermal collector. An iterative program was developed on MATLAB software that derived the temperatures of all the collector components iteratively. The obtained results, from the mathematical model, successfully predicted the collector's performance and four different cases of collector configuration were comparatively analyzed. It was observed that in case of evacuated configuration, when there is no natural convective heat transfer from the top of the absorber plate, collector top heat loss coefficient reduced from 5.35 W/m^2 K to 4.11 W/m^2 K. Enhancement in thermal efficiency and rise in outlet air temperature was observed in Case 3 & Case 4. Analysis of the results also showed that as the length of the collector is increased, air outlet temperature along with absorber plate temperature rises and consequently, PV module bonded to absorber plate at the outlet end will experience the lowest cell efficiency due to higher temperatures and module-absorber bonding and PV module itself will degrade faster due to higher temperatures. An improved overall efficiency of 67.3% has been achieved for EFPVT collector configuration.

Authors' Contributions

A Waqas supervised the project and provided conceptual guidance. I A Qureshi performed the literature review, and developed the mathematical model and computer code. I A Qureshi and A Waqas investigated and explained the obtained results. I A Qureshi wrote the paper. A Waqas reviewed and revised the final draft.

Refereces

[1] E. Radziemska, "The effect of temperature on the power drop in crystalline silicon solar cells," vol. 28, pp. 1–12, 2003.

[2] R. K. Koech, H. O. Ondieki, J. K. Tonui, and S. K. Rotich, "A Steady State Thermal Model For Photovoltaic / Thermal (PV / T) System Under Various Conditions," vol. 1, no. 11, pp. 1–5, 2012.

[3] K. E. Amori and M. A. Abd-alraheem, "Field study of various air based photovoltaic / thermal hybrid solar collectors," *Renew. Energy*, vol. 63, pp. 402–414, 2014.

[4] S. Dubey, G. S. Sandhu, and G. N. Tiwari, "Analytical expression for electrical efficiency of PV/T hybrid air collector," *Appl. Energy*, vol. 86, no. 5, pp. 697–705, 2009.

[5] F. Leonforte and C. Del Pero, "Modeling and Performance Monitoring of a Photovoltaic – Thermal (PVT) Water Collector," *Sol. Energy*, vol. 112, pp. 85–99, 2015.

[6] H. P. Garg and R. S. Adhikari, "Transient Simulation of Conventional Hybrid Photovoltaic / Thermal (Pv / T) Air Heating Collectors," vol. 562, no. February 1997, pp. 547–562, 1998.

[7] R. W. Moss, P. Henshall, F. Arya, G. S. F. Shire, T. Hyde, and P. C. Eames, "Performance and operational e ff ectiveness of evacuated fl at plate solar collectors compared with conventional thermal , PVT and PV panels," *Appl. Energy*, vol. 216, no. January, pp. 588–601, 2018.

[8] N. BENZ and T. BEIKIRCHER, "HIGH EFFICIENCY EVACUATED FLAT-PLATE SOLAR COLLECTOR FOR PROCESS STEAM PRODUCTION1Paper presented at the ISES Solar World Congress, Taejon, South Korea, 24–29 August 1997.1," *Sol. Energy*, vol. 65, no. 2, pp. 111–118, 1999.

[9] J. Watmuff and D. Proctor, "Solar and wind induced external coefficients - Solar collectors," no. May, 2017.

[10] M. H. Unsworth and J. L. Monteith, "Long□wave radiation at the ground I. Angular distribution of incoming radiation," *Q. J. R. Meteorol. Soc.*, vol. 101, no. 427, pp. 13–24, 1975.

[11] A. Tiwari and M. S. Sodha, "Performance evaluation of solar PV/T system: An experimental validation," *Sol. Energy*, vol. 80, no. 7, pp. 751–759, 2006.

[12] J. P. Holman, "Heat Transfer (10th Edition)," *McGraw-Hill Co.*, 2010.

[13] L. W. Florschuetz, "On heat rejection from terrestrial solar cell arrays with sunlight concentration," in *11th photovoltaic specialists conference*, 1975, pp. 318–326.

[14] T. T. Chow, "A review on photovoltaic / thermal hybrid solar technology," *Appl. Energy*, vol. 87, no. 2, pp. 365–379, 2010.

[15] I. H. Bell, J. Wronski, S. Quoilin, and V. Lemort, "Supporting Information to Pure- and Pseudo-Pure Fluid Thermophysical Property Evaluation and the Open-Source Thermophysical Property Library CoolProp Pure and Pseudo-pure fluids Incompressible liquids , aqueous solutions and slurries," pp. 1–14.